Factors controlling the distribution of ozone in the West African lower troposphere during the AMMA (African Monsoon Multidisciplinary Analysis) wet season campaign

Saunois M., Reeves C.E., Mari C.H., Murphy J.G., Stewart D.J., Mills G.P., Oram D.E., Purvis R.M.

Atmos. Chem. Phys., 9, 6135–6155, 2009
www.atmos-chem-phys.net/9/6135/2009/

Atmospheric Chemistry and Physics

Factors controlling the distribution of ozone in the West African lower troposphere during the AMMA (African Monsoon Multidisciplinary Analysis) wet season campaign

M. Saunois[1,2], C. E. Reeves[3], C. H. Mari[1,2], J. G. Murphy[3,4], D. J. Stewart[3], G. P. Mills[3], D. E. Oram[3], and R. M. Purvis[5,*]

[1]Université de Toulouse, UPS, LA (Laboratoire d'Aérologie), 14 avenue Edouard Belin, 31400 Toulouse, France
[2]CNRS, LA (Laboratoire d'Aérologie), 31400 Toulouse, France
[3]School of Environmental Sciences, University of East Anglia, Norwich, UK
[4]Department of Chemistry, University of Toronto, Toronto, Canada
[5]Facility for Airborne Atmospheric Measurement, National Centre for Atmospheric Science, Cranfield, UK
[*]now at: Facility for Ground Atmospheric Measurements, National Centre for Atmospheric Science, University of York, Heslington, York, UK

Received: 6 January 2009 – Published in Atmos. Chem. Phys. Discuss.: 16 March 2009
Revised: 1 July 2009 – Accepted: 13 July 2009 – Published: 27 August 2009

Abstract. Ozone and its precursors were measured on board the Facility for Airborne Atmospheric Measurements (FAAM) BAe 146 Atmospheric Research Aircraft during the monsoon season 2006 as part of the African Monsoon Multidisciplinary Analysis (AMMA) campaign. One of the main features observed in the west African boundary layer is the increase of the ozone mixing ratios from 25 ppbv over the forested area (south of 12° N) up to 40 ppbv over the Sahelian area. We employ a two-dimensional (latitudinal versus vertical) meteorological model coupled with an O_3-NO_x-VOC chemistry scheme to simulate the distribution of trace gases over West Africa during the monsoon season and to analyse the processes involved in the establishment of such a gradient. Including an additional source of NO over the Sahelian region to account for NO emitted by soils we simulate a mean NO_x concentration of 0.7 ppbv at 16° N versus 0.3 ppbv over the vegetated region further south in reasonable agreement with the observations. As a consequence, ozone is photochemically produced with a rate of 0.25 ppbv h^{-1} over the vegetated region whilst it reaches up to 0.75 ppbv h^{-1} at 16° N. We find that the modelled gradient is due to a combination of enhanced deposition to vegetation, which decreases the ozone levels by up to 11 pbbv, and the aforementioned enhanced photochemical production north of 12° N. The peroxy radicals required for this enhanced production in the north come from the oxidation of background CO and CH_4 as well as from VOCs. Sensitivity studies reveal that both the background CH_4 and partially oxidised VOCs, produced from the oxidation of isoprene emitted from the vegetation in the south, contribute around 5–6 ppbv to the ozone gradient. These results suggest that the northward transport of trace gases by the monsoon flux, especially during nighttime, can have a significant, though secondary, role in determining the ozone gradient in the boundary layer. Convection, anthropogenic emissions and NO produced from lightning do not contribute to the establishment of the discussed ozone gradient.

Correspondence to: M. Saunois
(marielle.saunois@aero.obs-mip.fr)

1 Introduction

One of the objectives of the African Monsoon Multidisciplinary Analyses (AMMA) project is to improve understanding of factors controlling the ozone concentrations over West Africa. This paper addresses this for the lower troposphere by using a two-dimensionnal (2-D) coupled chemistry dynamics model, the results of which are compared to concentration fields observed by a research aircraft.

Tropospheric ozone, O_3, is formed by photochemical oxidation of carbon monoxide (CO) and hydrocarbons in the presence of nitrogen oxides (NO_x). The formation of the hydroxyl radical, OH, by ozone photolysis is promoted in the tropics by high ultra violet (UV) radiation and temperature (Thompson, 1992). OH is the primary oxidant of the atmosphere and is responsible for the removal of many pollutants. In Africa primary pollutants come from biomass burning, natural emissions (e.g. vegetation, soils), lightning NO_x emissions and anthropogenic sources. These trace gases have a significant impact on atmospheric chemistry and can lead to formation of ozone.

African biomass burning results from agricultural practices and takes place during the dry season (Jonquière et al., 1998) contributing a large amount of the global emissions of CO, hydrocarbons and NO_x. During the monsoon (June, July and August) little biomass burning takes place over West Africa. However, biomass burning plumes from the Southern Hemisphere may be transported over the Atlantic Ocean to the Northern Hemisphere over West Africa (e.g., Jonquière et al., 1998; Sauvage et al., 2005, 2007b). Signatures of biomass burning plume intrusions have been observed during the AMMA campaign by radiosondings in Cotonou (Mari et al., 2008; Thouret et al., 2009) and airborne measurements on several research aircraft (Reeves et al., 2009).

Vegetation releases vast quantities of diverse volatile organic compounds (VOCs) (Kesselmeier and Staudt, 1999) and isoprene is one of the most important (e.g., Guenther et al., 1995). The effect of biogenic emissions from vegetation on ozone formation has been investigated in previous studies using global models by Wang and Eltahir (2000) and Pfister et al. (2008). They found that adding biogenic emissions change ozone by up to 8 ppbv over West Africa. Using a global climate model, Aghedo et al. (2007) investigated the impact of biogenic trace gases (VOCs, CO and NO_x) emitted from Africa and showed that this is the most important African emission source affecting the total tropospheric ozone.

As a catalyst for the ozone formation, NO_x influences the oxidative capacity of the atmosphere. Biogenic emissions of nitric oxide (NO) from soils remain uncertain and are highly controlled by surface soil temperature and moisture as well as nitrogen content in the soil. Evidence of large emission pulses of NO from West African Sahel soils wetted after a dry period were observed during AMMA (Stewart et al., 2008, and references therein). Using satellite data Jaeglé et al. (2004) also showed that NO emitted from wetted soils can lead to a significant enhancement of NO_x concentrations over West Africa. Recent AMMA studies have linked the NO emission from wetted soils to ozone enhancement during the West African Monsoon (WAM) (July and August 2006) (Stewart et al., 2008; Delon et al., 2008).

The electrical activity associated with deep convective systems in the InterTropical Convergence Zone (ITCZ) (Christian et al., 2003) is a major source of NO in the upper tropical troposphere (Pickering et al., 1996; Bond et al., 2002; Labrador et al., 2005; Martin et al., 2007; Sauvage et al., 2007c) which has a large influence on the ozone distribution in the middle and upper troposphere (Martin et al., 2000; DeCaria et al., 2005, among others) due to its relatively long lifetime. Sauvage et al. (2007b) and Saunois et al. (2008) have studied the possible impact of lightning NO_x on the ozone meridional distribution in the upper troposphere over Africa. Deep convection causes entrainment of ozone precursors from the surface to the free troposphere (Lawrence et al., 2003) whilst downdrafts supply the planetary boundary layer (PBL) with O_3 rich air from aloft (Jacob and Wofsy, 1990). Consequently surface ozone might slightly increase due to lightning NO (Aghedo et al., 2007) and downdrafts of O_3-rich air.

In Africa anthropogenic emissions have a large spatial variability with South Africa, Nigeria and Egypt contributing the largest amounts (Aghedo et al., 2007). In the region of interest, West Africa, Nigeria is the country which contributes the most to anthropogenic emissions according to emission inventories. Anthropogenic release of trace gases has a strong local effect in highly populated cities (e.g., Lagos in Nigeria, Cotonou in Benin, Ouagadougou in Burkina Faso) where urban pollution severely affects population health (Baumbach et al., 1995; Fanou et al., 2006; Linden et al., 2008). Using a global climate model Aghedo et al. (2007) found an increase of surface ozone of about 2–7 ppbv in West Africa due to anthropogenic emissions during boreal summer with a maximum effect located in Nigeria.

The dry deposition of O_3 is one of the most important sinks for ozone in the boundary layer. Using a one dimensional photochemical model for the planetary boundary layer, Jacob and Wofsy (1990) found that O_3 losses *via* deposition to the canopy of an Amazon forest reached $-2.0\,\mathrm{ppbv\,day^{-1}}$ leading to a net loss of O_3 in the PBL during the wet season. The majority of O_3 flux experiments in Congo and in Amazonia were carried out during the dry season (Kirchhoff et al., 1988; Gregory et al., 1988; Andrea et al., 1992; Cros et al., 1992, 2000; Matsuda et al., 2006; Rummel et al., 2007). However a few continuous O_3 flux measurements above tropical forests during the wet season were reported as part of the Amazonian Boundary Layer Experiment (ABLE) 2B (Fan et al., 1990), the experiment of Matsuda et al. (2006) in Thailand and the EUropean Studies on Trace gases and Atmospheric CHemistry as a contribution to the Large-scale Biosphere-Atmosphere experiment in Amazonia (LBA-EUSTACH) (Rummel et al., 2007). The calculated ozone dry deposition velocities during the wet season in respective of the three previously mentioned studies were in the range of 0.26–1.28 $\mathrm{cm\,s^{-1}}$, 0.25–0.65 $\mathrm{cm\,s^{-1}}$ and 0.3–1.5 $\mathrm{cm\,s^{-1}}$ depending on time of day.

During the AMMA campaign, ozone and trace gas measurements were made on board five aircraft (Reeves et al., 2009). Among them, the Facility for Airborne Atmospheric Measurements (FAAM) BAe-146 flew over West Africa

from Niamey and sampled both the boundary layer and the free troposphere. Figure 1 shows the flights tracks on a vegetation map. The latitudinal variation of the land cover in West Africa (ocean/savanna/steppe/semi-desert/desert) leads to a latitudinal variation of biogenic emissions which can lead to horizontal gradients in trace gas concentrations in the lower atmosphere (Reeves et al., 2009). In particular, Reeves et al. (2009) note that on average there is little variability in the ozone, CO or water vapor concentrations with longitude at any altitude. The general zonal homogeneity results from the homogeneity in the vegetation cover and atmospheric circulation that redistribute the air.

In this context, a 2-dimensional model is a useful numerical tool to investigate the relative importance of different chemical and physical processes influencing ozone and its precursors mixing ratios. Based on the zonal homogeneity in surface features, such as precipitation, vegetation, surface temperature and albedo over West Africa between 10° W and 10° E, a 2-D model has been developed by Peyrillé et al. (2007) to simulate a typical July monsoon regime in a latitude-altitude cross section. This idealized model has already been used for chemical modelling to study the impact of the lightning NO_x on the O_3 meridional profile in the upper troposphere (Saunois et al., 2008).

The FAAM BAe-146 flights were conducted between 4° W and 6° E. Therefore we will average natural and anthropogenic emissions between 5° W and 5° E to derive their mean latitudinal variatation. As a consequence, the model simulations represent a substantial and typical part of West Africa and we will denote in the manuscript the area between 5° W and 5° E as "West Africa".

Section 2 presents a brief description of the measurements made to obtain the observed data used in this study. Section 3 describes the 2-D idealized model along with the surface emissions and dry deposition velocities employed. Section 4 compares modelled and observed trace gases mixing ratios in altitude-latitude cross sections. The distribution of trace gases in the lowest 700 m of the atmosphere is discussed in Sect. 5. Section 6 presents different sensitivity tests to investigate the influence of dry deposition and emission sources on the ozone distribution.

2 Experimental data

The measurements used in this study were made onboard the FAAM BAe-146 Atmospheric Research Aircraft which was based in Niamey, Niger for the AMMA campaign from 17 July to 17 August 2006. Flights were conducted in a region from 4° N to 18° N and 4° W to 6° E over West Africa, mainly over Benin and south-west of Niger, as well as regions of Mali, Burkina Faso and Togo (Fig. 1). The flights sampled both the boundary layer and the free troposphere. A summary of the measurements including measured parameters, precision, accuracies and detection limits is given in Table 1. NO_x was measured using a commercial TECO 42C chemiluminescence NO_x analyser (hereafter referred to as the TECO NO_x instrument), which measures NO from the chemiluminescence of reaction with ozone. NO_2 (and some other NO_y species) are converted to NO by a molybdenum converter. Ozone was measured using a TECO 49C UV photometric instrument. Carbon monoxide was measured by Vacuum Ultra Violet (VUV) resonance fluorescence using an Aero Laser AL5002 Fast Carbon Monoxide Monitor (Gerbig et al., 1999). Isoprene, acetone and the sum of methacrolein and methyl vinyl ketone were measured using a Proton Transfer Mass Spectrometer (PTrMS) supplied by Ionicon Analytik (Murphy et al., 2009). The technique is based on the transfer of a proton from H_3O^+ to organic compounds which have a higher proton affinity. The resulting ions are detected using mass spectrometry. The instrument produced a point (1–2 s) measurement for each species of interest approximately every 15 s. Formaldehyde was measured using a fluorescence technique based on the Hantzsch reaction (Cardenas et al., 2000).

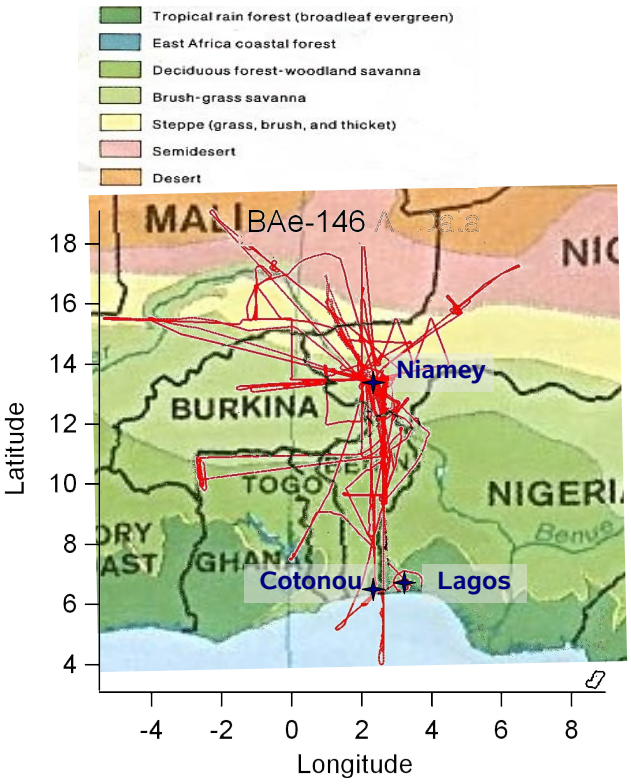

Fig. 1. Flights tracks of the BAe-146 (red lines) on a vegetation map.

3 Model description

The idealized 2-D version of the Méso-NH model used for this study was initially designed by Peyrillé et al. (2007)

Table 1. Measurements made on the FAAM BAe-146 Atmospheric Research Aircraft during AMMA used in this paper.

Species/Parameters	Reference	Technique	Averaging time	Accuracy	Precision	Detection limit
O_3	–	UV[1]	3 s	5%	1 ppbv	2 ppbv
CO	Gerbig et al. (1999)	VUV[2] fluorescence	1 s	–	1 ppbv	2 ppbv
Oxygenates	Murphy et al. (2009)	PTR-MS	1–2 s	10–50%	10%	20–80 pptv
NO_x	–	TECO	1 s	50 ppt	–	50 ppt
CH_2O	Cardenas et al. (2000)	Fluorometric	10 s	30%	12%	50 pptv

[1] Ultra Violet
[2] Vacuum Ultra Violet

to provide a latitudinal representation of the monsoon system and the associated circulation between 10° W and 10° E. Based on a similar 2-D approach Saunois et al. (2008) studied the budget of ozone in the upper troposphere. The model is based on the French community atmospheric simulation system Méso-NH (Lafore et al., 1998).

3.1 Model configuration

The 2-D model of Peyrillé et al. (2007) extends from 30° S to 40° N with a horizontal resolution of 70 km. The vertical domain extends to 20 km, with a variable grid-box height, which is about 30 m near the surface and 1 km in the upper troposphere. A so-called sponge layer above 20 km is implemented as an upper boundary to prevent wave-reflection at the top. The lateral boundary conditions applied to the North and South of the domain allow tangential velocities but introduce zero forcing so that no interaction with the mid-latitudes is allowed. The West African subcontinent is approximated as a flat continental band between 5° N and 30° N. Orographically induced circulation is thus not considered. Peyrillé et al. (2007) have shown that adding a plateau induces a northward displacement of the monsoon of about 3°. The convection parameterization from Bechtold et al. (2001) is adopted and includes transport and scavenging of soluble species (Mari et al., 2000). Turbulent processes are represented by the one-dimensional version of the turbulent scheme of Cuxart et al. (2000) which is based on the mixing length of Bougeault and Lacarrère (1989) and includes a prognostical turbulent energy equation. Atlantic Ocean and Mediterranean Sea surface temperatures (SST) are taken from the Reynolds climatology of 1982–2003 (Reynolds and Smith, 1995). We use July SST profiles for the Gulf of Guinea and May SST profiles for the Mediterranean Sea. The role of the SSTs in the Mediterranean Sea has been discussed by Peyrillé et al. (2007). The flux parameterization over the ocean for tropical winds is implemented according to Mondon and Redelsperger (1998). The exchange between the surface and the atmosphere is described by the Interactions between Soil, Biosphere and Atmosphere (ISBA) scheme of Mahfouf and Noilhan (1996).

Table 2. Description of some of the lumped species used in the ReLACs chemical mechanism and mentioned in this study. See Crassier et al. (2000) for further details.

ReLACS lumped species	Brief description
ETH	ethane
ALKA	alkanes, alkynes, alcohols, esters...
ALKE	ethene and higher alkene
BIO	isoprene + α-pinene + d-limonene ...
HCHO	formaldehyde
ALD	acetaldehyde and higher saturated aldehydes
KET	acetone and higher saturated ketones
CARBO	other carbonyls (among them: methacrolein..)
PAN	PAN, higher and unsaturated PANs
OP1	methyl hydrogen peroxide CH_3OOH
OP2	higher organic peroxides
MO2	Methyl peroxy radical
ALKAP	peroxy radical formed from ALKA
ALKEP	peroxy radical formed from ALKE
BIOP	peroxy radical formed from BIO
CARBOP	acetyl peroxy radicals (+ higher saturated and unsaturated) and peroxy radicals formed from KET

A reduced chemical scheme for tropospheric chemistry, the Regional Lumped Atmospheric Chemical Scheme (ReLACS, Crassier et al., 2000), has been added to the dynamical model. This chemical scheme is a reduced version of the explicit Regional Atmospheric Chemistry Mechanism (RACM, Stockwell et al., 1997). This reduced scheme was constructed following a "lumped molecule approach", in which the kinetic data and product yields for the lumped species (e.g. ALKA in Table 2) are calculated from the kinetic data and product yields of all primary species (e.g. alkanes, alkyns, alcohols...) using emissions rates and reactivity as weighting factors. ReLACS considers 37 chemical species and 128 equations. Table 2 summarises the correspondence between some lumped species and the actual chemical species that they represent. Under this assumption, an emitted species can be represented by a lumped species

Table 3. Surface emission fluxes in molecules cm^{-2} s^{-1} assigned in the model. Model species names are capitalized. Numbers in parentheses correspond to aggregation factors used to combine actual chemical species. See text for details.

Source	Ocean[a]	Vegetation	Soils		Anthropogenic[d]	
Location	<5° N & >30° N	5° N–12° N	5° N–12° N	12° N–16° N	5° N–8° N	8° N–14° N
CO	0.29E10	0.17E12[a]	0	0	0.51E12	0.11E12
NO_x	0	0	0.17E11[a]	0.45E11[c]	0.12E11	0.25E10
BIO						
isoprene (1)	0	0.22E12[b]	0	0	0	0
terpenes (1)	0	0.22E11[b]	0	0	0	0
ETH	0.13E9	0.99E9[a]	0	0	0.39E10	0.94E9
ALKA						
propane (0.44)	0.12E9	0.13E10[a]	0	0	0.13E10	0.34E9
butane (0.85)	0	0	0	0	0.20E10	0.54E9
higher alkanes (1.20)	0	0	0	0	0.37E10	0.60E9
methanol (0.38)	0	0.75E11[a]	0	0	0	0
alcohols RETRO (lumped)	0	0	0	0	0.75E10	0.18E10
ethyne (0.31)	0	0	0	0	0.30E10	0.70E9
ALKE						
ethene (0.96)	0.20E9	0.53E10[a]	0	0	0.72E10	0.17E10
propene (1.04)	0.15E9	0.71E9[a]	0	0	0.21E10	0.51E9
KET						
acetone (0.33)	0	0.15E9[a]	0	0	0.11E10	0.28E9
HCHO	0	0	0	0	0.12E10	0.28E9
ALD	0	0	0	0	0.22E10	0.52E9

[a] Adapted from the POET/GEIA inventory
[b] Adapted from MEGAN/MOHYCAN (Müller et al., 2008)
[c] Adapted from Jaeglé et al. (2004)
[d] Adapted from the RETRO 2000 inventory (Schultz et al., 2005)

which reacts at a different rate providing that an aggregation factor is applied to the compound emissions. These aggregation factors can be seen in the Table 3 where emission fluxes are summarised. For example, for the lumped species called ALKA, the emission of ALKA is equal to 0.44 times the emission of propane plus 0.38 times that of methanol.

A parameterization of the NO_x production by lightning (LNO_x) has been implemented into the deep convection scheme by Mari et al. (2006). The parametrization of the lightning frequency is based on Price and Rind (1992) and related to the convective cell height. The ratio IC/CG (IC stands for Intra-Cloud and CG for Cloud-to-Ground lightning) is derived from Price and Rind (1993) and depends on the depth of ice layers in the cloud. The NO production in the flashes is assumed to be proportional to air density along the flash. The feature of this scheme is that it uses updraft and downdraft mass fluxes modelled by the deep convection scheme to generate the profile of lightning NO_x. The LNO_x source is calibrated to 25 Mg(N)/month to obtain simulated ozone and NO_y mixing ratios in agreement with the measurements made on board the MOZAIC aircraft (Saunois et al., 2008).

The model is initialised with a quiet, horizontally homogeneous and almost dry (10% relative humidity) atmosphere. For initialisation, the mixing ratios of the chemical species were set to constant values (50 ppbv for O_3, 100 ppbv for CO, 10 pptv for NO and NO_2 and 1 pptv the others species). The model was then integrated for 30 days, with solar conditions corresponding to a permanent day choosen as the 15th July, and includes diurnal variations. 10 to 15 days spin-up are needed for the model to develop a deep convectiion zone. The trace gases distributions show little day-to-day variations after 25 days of simulation and the influence of the initial concentrations of trace gases was found to be negligible after 25 days of simulation.

3.2 Surface emissions

Table 3 summarises the set of surface emissions used in this study. Surface emission variations follow the latitudinal land cover as observed during the period of measurements so that the model can closely reproduce the observed distribution of ozone and its precursors. As a consequence of the model configuration, ocean is considered south of 5° N and north of 30° N. Isoprene is known to be emitted from trees and satellite data of leaf area index and visual observations from the

research aircraft during AMMA showed tree cover to extend from the coast to 12–13° N. From 12–13° N to the limit of the desert (16° N) was mostly bare soil. Consequently emissions from vegetation are considered between 5° N and 12° N in the idealized model and NO emission from soil between 5° N and 16° N. Because of the canopy reduction south of 12° N and the NO pulses over bare soils caused by the numerous precipitation events at this time of the monsoon (Stewart et al., 2008; Delon et al., 2008), the rates of NO emissions are lower south of 12° N than between 12 and 16° N.

Müller et al. (2008) have recently calculated isoprene emission fluxes based on the MEGAN/MOHYCAN model. We used their estimate for July 2006 to derive our isoprene emission rate. The terpene emissions are those of isoprene scaled by 0.1 (ratio derived from the analyse of the POET/GEIA emission rates in our domain of interest). The emissions rates for the remaining biogenic compounds have been derived from the estimate of the POET/GEIA inventory (Granier et al., 2005) for July 2000. For soil NO_x emission, we use the POET/GEIA inventory (Granier et al., 2005) and the work of Jaeglé et al. (2004) to derive fluxes south and north of 12° N, respectively. The biogenic emission rates shown in Table 3 are mean values over the longitudinal band 5° W–5° E between 30° S and 5° N, 5° N and 12° N and 12° N and 16° N for ocean, vegetation and wetted bare soils areas, respectively. A set of anthropogenic emissions is included as well. We use the RETRO 2000 inventory (Schultz et al., 2005) to derive the average anthropogenic emission fluxes between 5° W and 5° E. This inventory includes different sectors of activity (power generation, residential, commercial and other combustion, industrial combustion, road transport and ships). The latitudinal distribution of anthropogenic emissions shows higher values to the south due to higher population density near the coast. As a consequence, a two-step distribution is applied with high (low) values derived from the calculated mean between 5° N and 8° N (8° N and 14° N). Except for emissions from vegetation, which have a diurnal variation with a maximum at 12:00 UTC, the emission fluxes are kept constant throughout the simulation.

3.3 Dry deposition velocities

Table 4 summarises the dry deposition velocities used in this study. Velocities for dry deposition also follow the latitudinal land cover but, unlike reality, they do not have diurnal variations. Deposition velocities for NO, NO_2, HNO_3, H_2O_2 were adopted from Seinfeld and Pandis (1998) and for HCHO, aldehydes, PAN from von Kuhlmann et al. (2003). The dry deposition velocity for ozone over ocean and desert is taken from Seinfeld and Pandis (1998). For ozone dry deposition over vegetation, the value of 0.65 cm s^{-1} is taken from Matsuda et al. (2006) who studied the ozone dry deposition over tropical forest in Thailand during the wet season. This value is in the range of the ones calculated by Rummel et al. (2007) from the LBA-EUSTACH 1 experiment during the wet season in Amazonia which vary between around 1.2 cm s^{-1} during daytime to 0.3 cm s^{-1} during nightime leading to a 24 h average velocity of 0.67 cm s^{-1} above canopy.

Table 4. Dry deposition velocities in cm s^{-1} adopted from Seinfeld and Pandis (1998) for NO, NO_2, HNO_3, H_2O_2 and from von Kuhlmann et al. (2003) for HCHO, OP1 (CH_3O_2H) and PAN. O_3 deposition velocities are taken from Seinfeld and Pandis (1998) over ocean and desert, and from Matsuda et al. (2006) over vegetation.

Ocean	Vegetation	Desert	Bare soil
O_3	0.07	0.65	0.1
NO	0.003	0.016	0.003
NO_2	0.02	0.1	0.02
H_2O_2	1.0	0.5	1.0
HNO_3	1.0	4.0	1.0
HCHO	0.9	0.36	0.36
OP1	0.35	0.18	0.18
PAN	0.02	0.1	0.1

4 Meridional distribution of ozone and its precursors in the lower troposphere

A reference run (named BASE) which includes all the surface sources (biogenic and anthropogenic) as well as lightning emission of NO, was performed. Figure 2 to Fig. 7 shows the latitude-altitude cross sections of simulated and observed trace gases. The simulated values are average concentrations over the last five days of simulation. The observed data are the averages from all the BAe-146 flights that took place between the 20th July and the 17th August 2006.

4.1 Hydrocarbons

BIO is the lumped species for isoprene and terpenes (Table 2) and its emissions correspond to 91% of isoprene and 9% of other terpenes (Table 3). Figure 2a and e show the observed isoprene and simulated BIO cross sections. Similar to isoprene, BIO remains close to the vegetation sources due to its short lifetime. The typical lifetime of BIO at 12:00 UTC for its reaction with OH is 1.5 h in the lowest levels of the model and 30–45 min at 1 km reflecting the vertical gradient of OH south of 12° N (Fig. 7). The BIO lifetime is also affected by its reaction with O_3 (1–1.5 days at 12:00 UTC). The longer lifetime of BIO near the surface favours a vertical mixing up to 1–2 km. At this altitude, BIO is rapidly oxidized as also found by Jacob and Wofsy (1990) in the Amazonian PBL during the wet season. At 500 m, the simulated BIO mixing ratio (Fig. 2a) ranges between 0.7 and 1.0 ppbv in good agreement with the observed isoprene mixing ratios at the same altitude (Fig. 2e). CARBO is a lumped species for glyoxal and other carbonyls, including

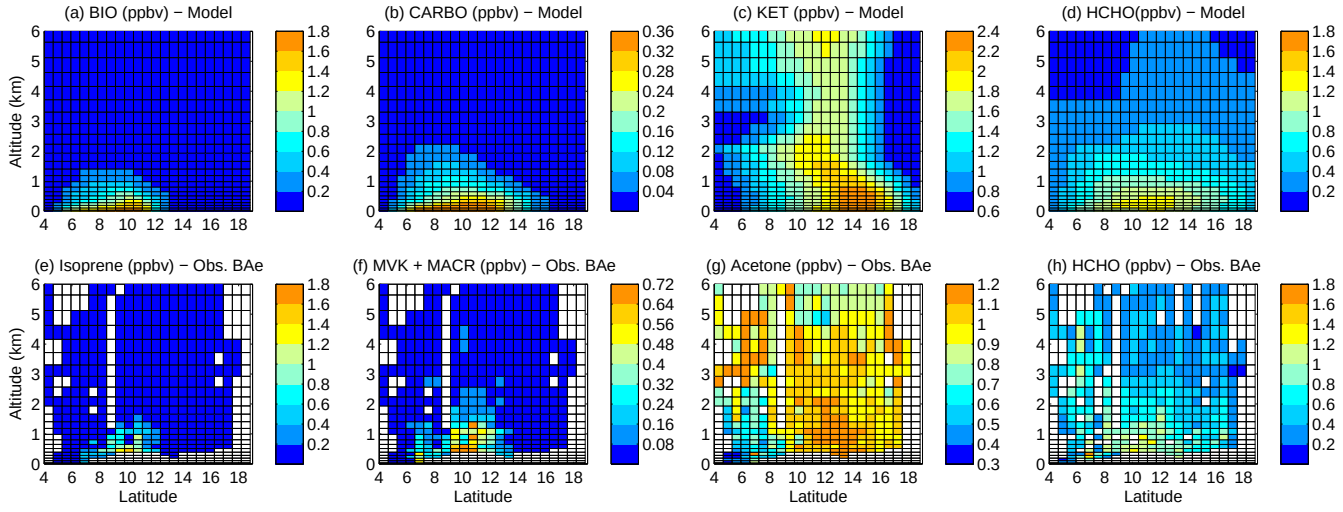

Fig. 2. Meridional vertical cross sections of the simulated BIO, CARBO, KET and HCHO (top) in ppbv between 4° N and 19° N from the surface up to 6 km. They are compared with their respective comparable observed species (bottom) which are isoprene, MVK+MACR, acetone and HCHO, respectively. The simulated values are average concentrations over the last five days of simulation. The observed data are the averages from all the BAe-146 flights that took place between 20th July and the 17th August 2006.

methacrolein (Table 2), and is essentially a product of the BIO oxidation. Its lifetime with respect to reaction with OH is longer than that of BIO (around 10 h near the surface and 2–3 h at 1 km) and allows it to be transported slightly further upwards and northwards (Fig. 2b). CARBO is initially produced within the lowest levels of the model but is rapidly oxidized above about 500 m and north of 12° N. Comparing the simulated concentrations of CARBO with the observations is not straightforward because not only does CARBO represents many compounds, but the PTr-MS measurements of methacrolein (MACR) cannot be separated from that of methyl vinyl ketone (MVK), which is not represented by CARBO. Despite this the measured MVK+MACR and simulated CARBO both show very similar distributions (Fig. 2b and f) which are slightly more widespread in altitude and latitude than the observed isoprene and simulated BIO. A quantitative comparison is unfortunately inappropriate between CARBO and MVK+MACR.

KET, the lumped species for ketones, is treated chemically as 50% acetone and 50% MVK (Stockwell et al., 1997). Here again comparing measurements with model results is rather difficult. However the simulated KET distribution has the same pattern as the observed acetone, both with maxima around 13–15° N (Fig. 2c and Fig. 2g), which is quite different from that of the MVK+MACR. The simulated mixing ratios for KET are twice those observed for acetone (e.g. near the surface around 15° N KET is simulated to be up to 2.6 ppbv whereas observed acetone reaches only 1.3 ppbv). This is partly due to the lumped effect, but inaccuracies in emissions or the chemical scheme cannot be excluded.

The HCHO distribution is well simulated by the model with a northward extent to 17° N and a vertical extent up to 2 km (with concentrations up to 0.6 ppbv at 2 km). Near the surface, the simulated HCHO mixing ratios range between 0.8 and 1.4 ppbv in reasonable agreement with the observed values (Fig. 2d and h).

4.2 Carbon monoxide

Both observed and simulated CO mixing ratios show higher values south of 13° N and lower to the north (Fig. 3) below 2 km.

It is worth noting that the high concentrations of CO which were observed in the free troposphere above 2 km and south of 8° N are not reproduced by the model. Based on tracers such as acetonitrile and dispersion model calculations, it has been found that these polluted air masses have been impacted by biomass burning from the Southern Hemisphere (Mari et al., 2008; Janicot et al., 2008; Reeves et al., 2009). High concentrations of HCHO, NO_x and O_3 (Figs. 2b, 4b, 5b) at this altitude and latitude are signatures of this biomass burning pollution as well. This biomass burning pollution is not reproduced in the model because the biomass burning source is out of the bounds of our model domain.

Below 2 km, the model underestimates the CO mixing ratios compared to the BAe-146 measurements with only 120 ppbv as the maximum. The multimodel comparison of Shindell et al. (2006) shows that underestimation of CO is a common behaviour of atmospheric chemistry models in particular in the Northern Hemisphere extra-tropics. GEOS-Chem simulations of the tropical troposphere also underestimate CO in the African lower troposphere (Sauvage et al.,

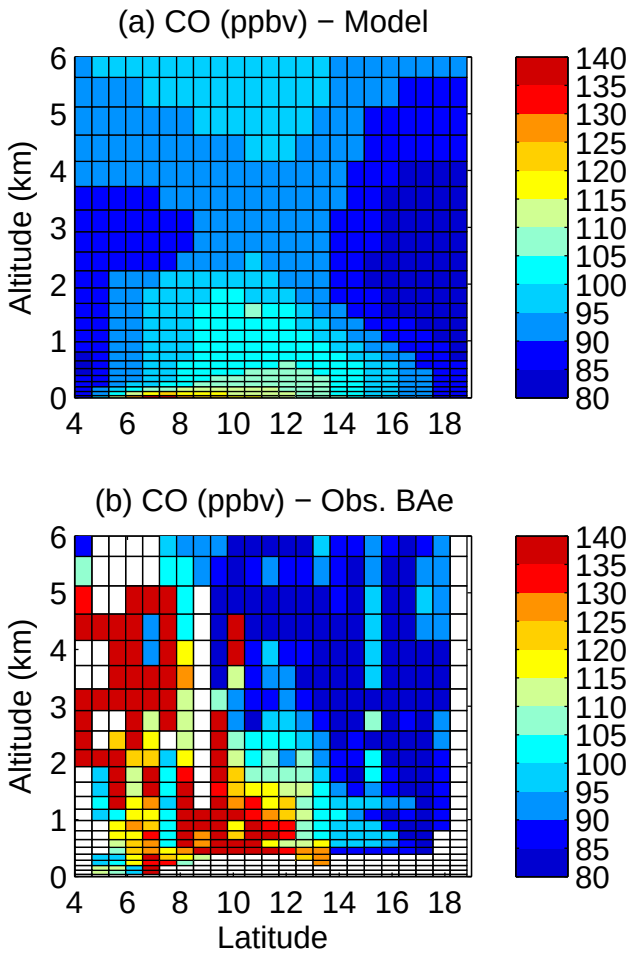

Fig. 3. Same as Fig. 2 for the simulated **(a)** and observed **(b)** CO mixing ratios in ppbv.

2007a). The model underestimation in CO concentrations may be due to either underestimation of direct sources (anthropogenic or natural emissions) or secondary production from VOCs' oxidation (i.e. a chemical scheme issue). Jacob and Wofsy (1990) could not explain the CO enhancement in the Amazonian PBL by the oxidation of biogenic hydrocarbons. They showed that direct emissions from the forests account for 88% of the total modelled CO in the PBL. A sensitivity test detailed later in Sect. 6 shows that biogenic hydrocarbons oxidation accounts for around 10–15% of the total modelled CO below 700 m (NSVOC test of Sect. 6, Fig. 8). An artificial increase of OH concentration over vegetation (OHRE2 test of Sect. 6, Fig. 8) does not help to improve the CO comparison either. The results of the sensitivity tests suggest that the modelled CO amount is mainly driven by direct emissions and background methane oxidation in our model. In our model, we find a loss of CO by convective transport of CO-rich air out of the PBL. Photochemical production and loss of CO in the PBL are dependant on the altitude and latitude. Net photochemical production of CO takes place below 1–1.5 km and between 5° N and 13° N while net photochemical destruction of CO occurs elsewhere (not shown).

Increasing CO concentrations (through direct or indirect sources) might change ozone concentrations by a few ppbv but is expected to have an insignificant influence on the ozone gradient. The analyses of the CO distribution and budget in the African PBL is out of the scope of this study. Further investigations should be performed based on the aforementioned tests to improve the simulations of CO over West Africa.

4.3 Nitrogen oxides

Figure 4 shows the observed and simulated NO_x meridional distribution. The simulated NO_x mixing ratios are clearly controlled by the meridional gradient of the emission rates. The highest values of NO_x are found north of 12° N (with concentrations up to 1 ppbv near the surface) where emission rates from bare soils have been assumed to be higher. At 500 m altitude, the simulated NO_x concentrations reach 500 ppt between 13° N and 17° N in good agreement with the observations. A secondary maximum near the surface is found around 7° N due to anthropogenic emissions. The observed surface NO_x mixing ratios show high values around urban areas (∼6.5° N for Cotonou and Lagos and ∼13° N for Niamey, see the map Fig. 1). This local effect is smoothed by the model due to the idealized variation of emissions and the coarse horizontal resolution of the model (70 km). The high values of NO_x observed south of 6° N at 2–5 km (Fig. 4b) are signatures of the biomass burning plume intrusions from the Southern Hemisphere.

4.4 Ozone

Figure 5 presents the observed and simulated ozone distributions. The observed distribution of O_3 is characterized by a vertical gradient with lower values in the boundary layer and a strong meridional gradient at 14° N below 2 km. These patterns are well reproduced by the model. Lower values of O_3 below 2 km and south of 13° N are well captured by the model and range between 20 and 30 ppbv in reasonable agreement with the observations. Janicot et al. (2008) and Reeves et al. (2009) suggested that these lower values south of 13° N are partly due to rapid deposition to trees. Mixing ratios up to 40 ppbv are obtained in the boundary layer around 15–16° N in both the model and observations. In the middle troposphere, the high O_3 values observed at 2–5 km at 4–8° N correspond to the biomass burning plume previously mentioned.

The simulated distributions of O_3 in the PBL is regulated by three main processes: a downward transport from the free tropopshere, deposition to the surface (especially over vegetation) and photochemistry. Figure 6 presents the vertical cross-section of the convective and chemical tendencies of ozone during daytime. The ozone convective tendency in

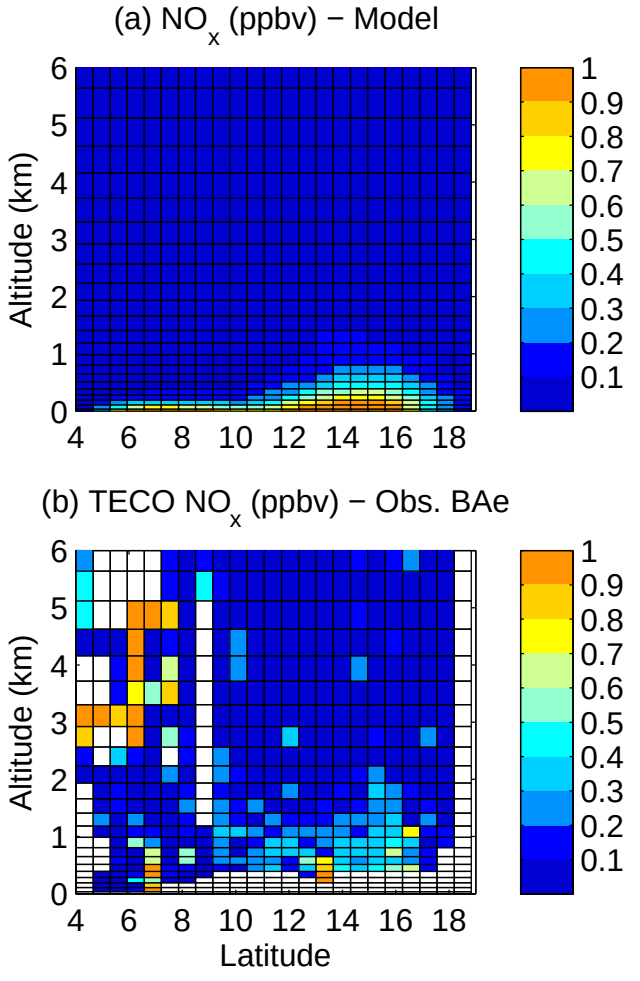

Fig. 4. Same as Fig. 2 for the simulated **(a)** and observed **(b)** NO_x mixing ratios in ppbv.

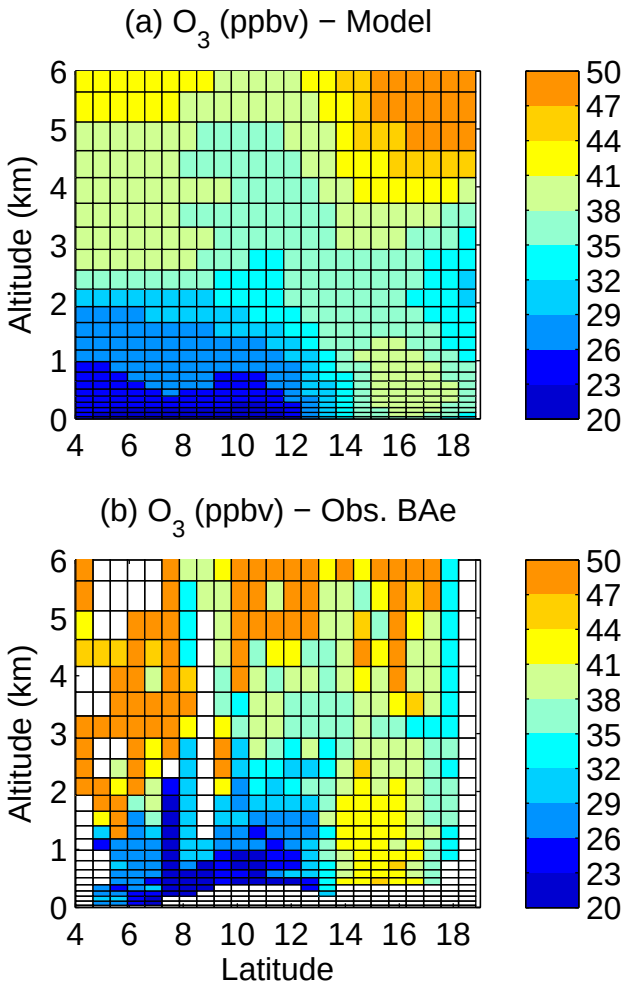

Fig. 5. Same as Fig. 2 for the simulated **(a)** and observed **(b)** O_3 mixing ratios in ppbv.

the PBL is positive showing that convection acts as a source of ozone through downward transport from the free troposphere. Photochemical production and loss of O_3 in the PBL is strongly dependant on altitude, latitude and time. During daytime, net photochemical destruction of O_3 takes place above 1200 m while net photochemical production (Fig. 6) occurs in the lowest levels of the model where the NO concentration is higher (Fig. 4). Comparing the reaction rates of the peroxy radicals with HO_2 against those with NO at 12:00 UTC, we find that the peroxy radicals preferentially react with HO_2 above 1 km while their reactions with NO is favoured below 1 km in higher NO conditions. These latter reactions lead to the formation of NO_2 and then O_3. The threshold NO concentration for net photochemical O_3 production in the model depends on the latitude: 60 ppt of NO_x and 15 ppt of NO over vegetation, 100 ppt of NO_x and 30 ppt of NO north of 12° N. Below that threshold of NO concentration, O_3 is photochemically destroyed. Jacob and Wofsy (1990) found a threshold NO concentration of about 5 ppt over Amazonia during the wet season. The different VOC amounts available in the two experiments might explain the different thresholds. The O_3 production rate is a function of NO_x mixing ratio and reaches more than 0.6 (1.2) ppbv h^{-1} south (north) of 12° N. Jacob and Wofsy (1990) also simulated a production rate of O_3 of up to 0.5 ppbv h^{-1} in lower NO_x conditions.

4.5 Hydroxyl radical OH and HO_2

Figure 7 shows the modelled OH and HO_2 distributions on the 26th day of the simulation at 12:00 UTC. A sharp gradient of OH is simulated around 13° N. The much lower concentrations of OH south of 13° N are largely due to rapid loss by reaction with BIO over the vegetated region in the model. The simulated OH distribution is similar to that of O_3 in the PBL but the gradient of OH is sharper than the O_3 gradient. The modelled HO_2 distribution presents a similar pattern with higher values north of 13° N (6–

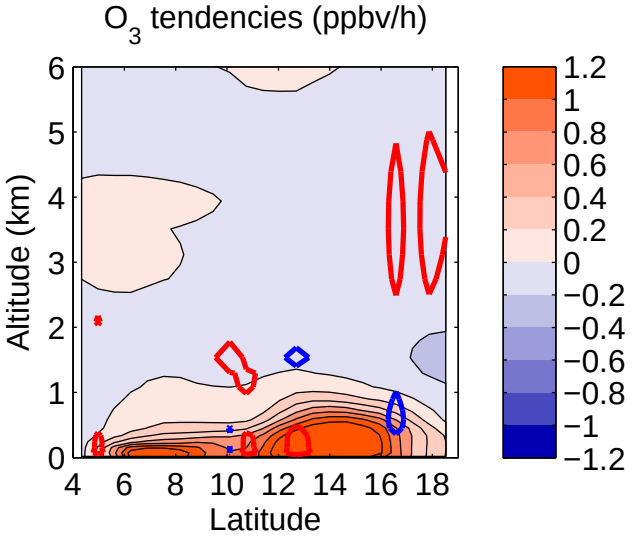

Fig. 6. Meridional vertical cross section of the simulated O_3 chemical tendency (coloured area) during daytime in ppbv h^{-1} between 4° N and 19° N from the surface up to 6 km. For the convective tendency, only the isolines at -0.5 ppbv h^{-1} (blue) and $+0.5$ ppbv h^{-1} (red) are plotted. The simulated values are averages over the last five days of simulation.

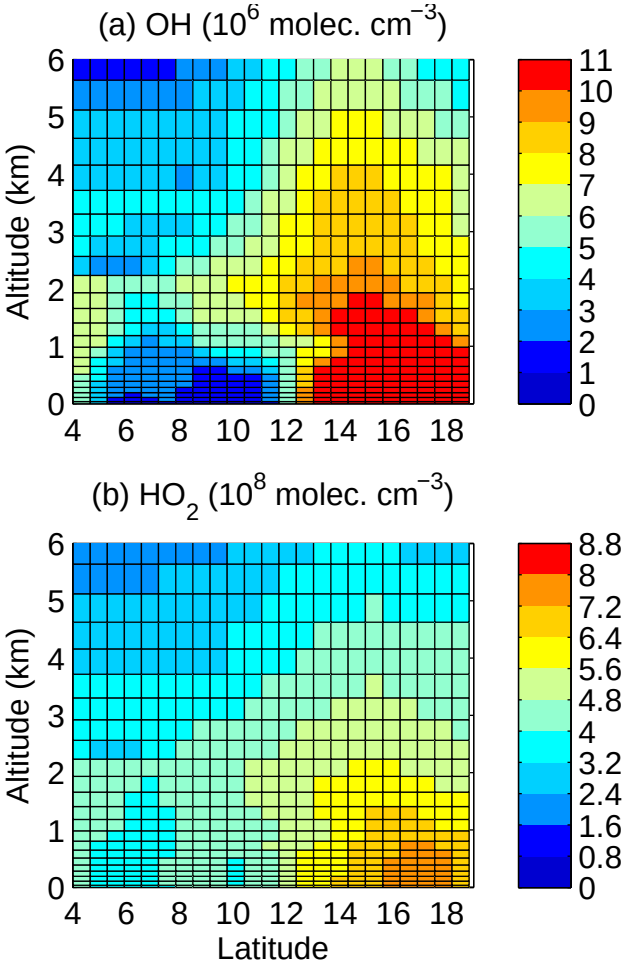

Fig. 7. Meridional vertical cross sections of OH (top) in 10^6 molecules cm^{-3} and HO_2 (bottom) in 10^8 molecules cm^{-3} between 4° N and 19° N from the surface up to 6 km simulated at 12:00 UTC the 26th day of simulation.

8×10^8 molecules cm^{-3}) compared to the southern concentration ($3–4\times10^8$ molecules cm^{-3}).

Unfortunately the diurnal variability in HO_x along with the spatial and temporal limitations of the measurements performed on board the BAe during AMMA makes it difficult to compare the modelled latitudinal distribution of HO_x with the observations. However some point to point comparisons between the model and the observations appear to suggest that the model might underestimate OH by a half over vegetation and overestimate HO_2 by $1–3\times10^8$ molecules cm^{-3} north of 12° N.

The low OH calculated by the model in the region of high isoprene concentration is typical of many models as discussed by Lelieveld et al. (2008). Here we address the influence of a possible misrepresentation of HO_x on the ozone and its precursors concentrations. This has been assessed through an artificial OH recycling within the reaction between isoprene peroxy radicals BIOP and HO_2 that leads to isoprene peroxides as suggested in Butler et al. (2008). The results of this test are shown in Fig. 8 using the meridional profiles of the trace gases below 700 m. Including this recycling increases the OH concentration over vegetation by a factor of 2–3, but this reduces the agreement with the observed concentrations of isoprene (Fig. 8a). This direct effect could be improved by reducing the reaction rate between OH and isoprene to take account of the artificial mixing of short-lived species in models of this grid size (Krol et al., 2000). However this substantial change in HO_x and isoprene induced only a small change in the PBL isoprene products (CARBO, KET and HCHO) and overall it led to insignificant changes in the ozone latitudinal distribution (Fig. 8g). These results suggest that the misrepresentation of HO_x, if there is any, will not alter the following discussion about the ozone distribution in the PBL.

5 Trace gas chemistry in the West African boundary layer (below 700 m)

The flights dedicated to the boundary layer survey were below 700 m and mostly between 300 and 600 m above sea level. The layer 0–700 m is mostly within the observed BL (Stewart et al., 2008) which is in agreement with the boundary layer height simulated by the model, diagnosed with the turbulent kinetic energy (0.7–2 km). In the following we focus on the layer below 700 m where most of the data were

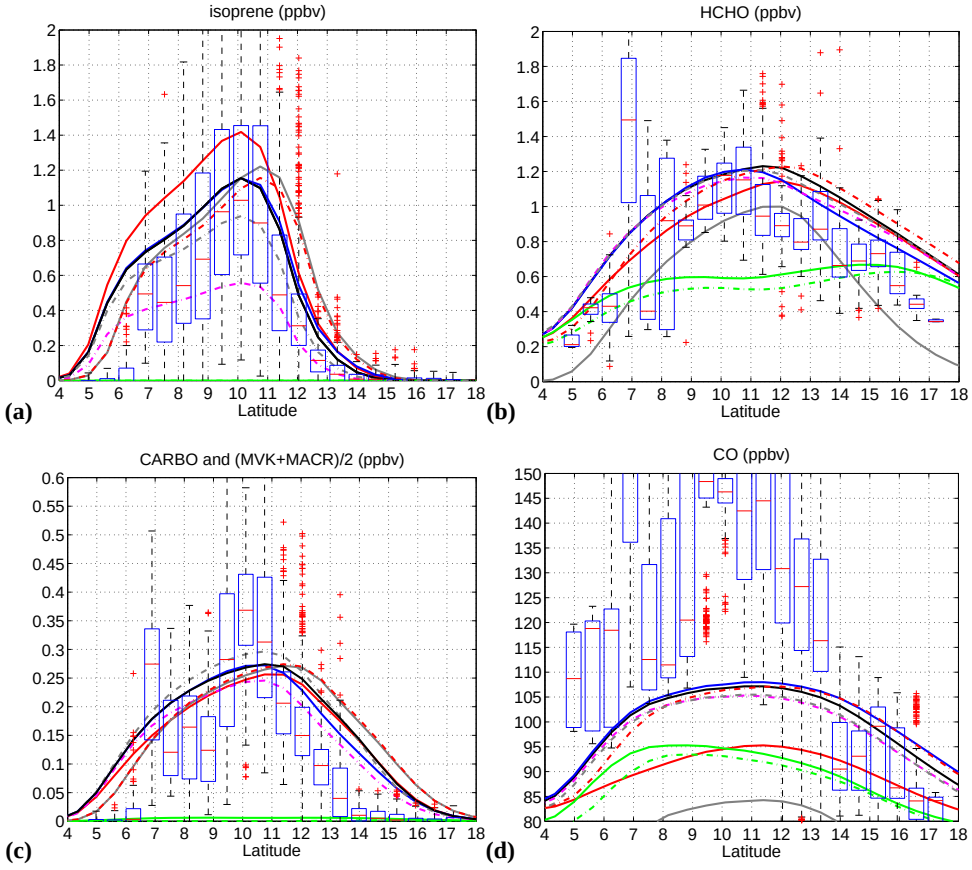

Fig. 8a. 24 h-average meridional profiles of BIO **(a)**, HCHO **(b)**, CO **(c)**, CARBO **(d)**, KET **(e)**, NO_x **(f)** and O_3 **(g)** in ppbv. The simulated mean profiles are calculated for the layer 0–700 m over the last five days of simulation for the BASE run (black line) and eight sensitivity tests (colored lines) (see the legend). The lumped species are compared to their respective comparable observed species which are isoprene, HCHO, CO, MVK+MACR, acetone and O_3, respectively. The observed values are the calculated means below 700 m and in the latitudinal bins of the model. They are presented using box and whisker plots. The red bar is the median, the blue bar the range of the 25 to 75 percentiles. The vertical black whiskers extent to the most extreme data values within 1.5 times the interquartile range of the box. The red crosses correspond to outliers with values beyond the ends of the whiskers.

collected and where the surface effects and the trace gas gradients are pronounced.

5.1 Trace gas meridional profiles below 700 m

Figure 8 compares the modelled meridional profiles of trace gases with the measurements. The measurements have been averaged for all locations within the latitudinal range of the horizontal grid boxes of the model and for all altitudes from the surface up to 700 m. The observed profiles (box and whisker plots) as well as the simulated profiles (solid or dashed lines) are presented in Fig. 8. The reference run is the black solid line and the other lines correspond to sensitivity tests discussed later in the paper.

As shown in Fig. 8a, the isoprene mixing ratios are captured well by the model species BIO between 8 and 11° N with values close to the median of the observations or inside the interquartile range. We see discrepancies outside this range where the model overestimates the isoprene mixing ratios, because emissions from vegetation are assumed to cover a broader latitudinal band of 5–12° N. The coast in the model is set at 5° N, which is typical for the southern coast of West Africa within the model domain, but the coast where the airborne measurements were made is located near 6° N. This explains the model overestimation seen around 5–6° N. The observations and the MEGAN/MOHYCAN model suggest also that emissions drop off towards the coast and become more patchy towards 12° N. The assumption of constant latitudinal average emissions from vegetation in the 5–12° N band may induce an overestimation of simulated BIO concentrations as well as HCHO, CARBO (compared to MVK+MACR) and CO concentrations (Fig. 8b, c, d) close to both sides of the vegetated area. The CO mixing ratio is largely underestimated south of 13° N as discussed previously. Close to ∼7° N and 13.5° N, the high measured concentrations of CO, HCHO and NO_x correspond to pollution from the cities of Lagos (Hopkins et al., 2009) or Cotonou,

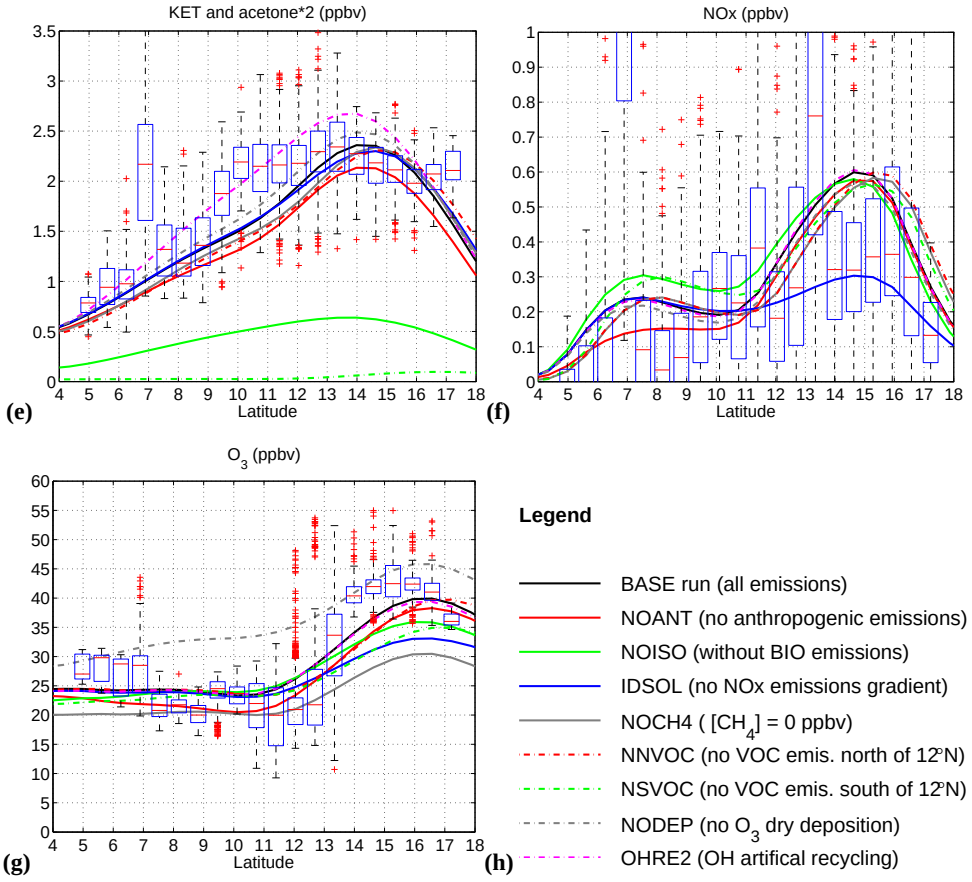

Fig. 8b. Continued.

and Niamey, respectively. CARBO and MVK+MACR do not compare well quantitatively, as discussed previously, but their meridional variations are reasonably similar given the latitudinal shift of the drop-offs resulting from the modelled BIO distribution described above. The acetone profile exhibits a much broader maximum than does KET.

The modelled NO_x agrees reasonably well with the measurements in that they are mostly within the interquartile range (Fig. 8f). It is, however, hard to discern a clear latitudinal gradient in the observations, partly because the data at ∼7° N and 13.5° N are skewed by pollution from the cities of Cotonou, Lagos and Niamey and partly because the data exhibit considerable variability due to large instrumental noise and to some extent atmospheric variability. The TECO NO_x instrument has a detection limit of 50 ppt with a 2 min averaging time while the data is reported as 10 s data leading to a detection limit of at least a few hundred ppt. By averaging over grid boxes we are considering enough data such that the median should be a reasonably robust value and give some indication of how NO_x varies with latitude. Another point is that the TECO NO_x measurements includes a fraction of NO_z(=NO_y-NO_x) (Stewart et al., 2008). To estimate this effect NO_x data from the FAAM TECO NO_x instrument was compared to data from the University of East Anglia NO_{xy} instrument which like the TECO instrument measures NO by chemiluminescence, but since it photolytically converts NO_2 to NO it should not measure NO_z. During AMMA on average NO_x data from TECO NO_x was about 16% higher than NO_x data from NO_{xy} instrument (Stewart et al., 2008). Unfortunately the NO_{xy} instrument was not operational on many flights so the data are too sparse to provide a good representation of the latitudinal gradient of NO_x which is why the data from the TECO instrument have been used. Given the uncertainty in the measurements, the modelled NO_x concentrations are in the range of observations, except south of 8° N where NO_x is overestimated . The simulated NO_x profile does not reproduced the spatial variability of the measurements due to the idealized emissions and exhibits too sharp a gradient between 12° N and 16° N.

As shown in Fig. 8g, the O_3 model to measurement comparison is rather good though it shows also a few discrepancies linked to points already mentioned for the VOCs and the NO_x. The O_3 values simulated in the reference run (black line) between 7 and 13° N are in reasonable agreement with measurements. The model fails to reproduce the higher values of O_3 south of 7° N probably because the misplaced coast induces an overestimated sink of O_3 through dry deposition. The model simulates the O_3 maximum 1° further north

compared to the observed maximum. This shift seems to be linked to the overestimation of VOCs north of 11° N. As a consequence, the O_3 production might be too efficient in the model north of this latitude. The model resolution is probably too coarse to expect a perfect agreement for the ozone maximum location. We found that the maximum can be shifted by ±1° in latitude by changing the vegetation northern limit in the model by 0.5–1°. Finally we notice that the simulated meridional gradient is not as sharp as the observed one.

Despite some discrepancies, the reasons for many of which are known and understood, the idealized 2-D model reproduces well the main trace gases variations. In the next two subsections, the trace gas transport during the night associated with northward advection and the O_3 distribution in the PBL are discussed.

5.2 Northward advection by the monsoon flux

Peyrillé and Lafore (2007) discussed the diurnal cycle of the West African monsoon dynamics as revealed by the 2-D model in a more developed configuration than the one used in Peyrillé et al. (2007) and here. In particular they found that the intensity of the monsoon wind reaches a maximum at around 02:00 UTC. This behaviour of the 2-D model agrees well with the diurnal cycle of the monsoon circulation as shown in numerical model analyses (ERA-40 from ECMWF or those of NCEP/NCAR) (Parker et al., 2005). In our model, the meridional wind is also strongest at night with an intensity of around 4–8 m s^{-1} below 700 m. This suggests that northward advection of materials is favoured during night-time. Long-lived species (relative to this transport) such as methane, CO and ozone, will be transported efficiently to the north. Also, after dark, the lifetimes of the pollutants such as isoprene and its oxidation products are longer because the concentrations of OH, which is the main oxidant, decrease. Consequently those more reactive species can also be transported north of the vegetated area where NO_x mixing ratios are higher. Figure 9 shows the diurnal cycle of the CARBO lumped species below 700 m. The northward advection of CARBO is seen in the non-zero concentration between 12 and 17° N. At these latitudes, the simulated meridional wind is up to 6 m s^{-1} during night-time so that the CARBO species can be transported by more than 1° in 5 h 30 min. Indeed, on 25 July 2006, an afternoon flight (B219A) which presented high biogenic emissions, was followed by a later flight (B219B) after dark. These companion flights aimed to study how the chemical composition evolved and how the nocturnal winds redistribute the air. During the night flight, biogenic species were observed north of the vegetated region, confirming a nocturnal advection of these species. A rough estimate of the northward wind during that night gives a value of around 4 m s^{-1}, in agreement with the simulated meridional wind in the model below 1 km. Consequently the northward advection by the monsoon winds could be a potential mechanism to transport trace gases, for instance reactive VOCs, to the NO_x-richer region. As a consequence the northward advection might influence the ozone distribution in the PBL.

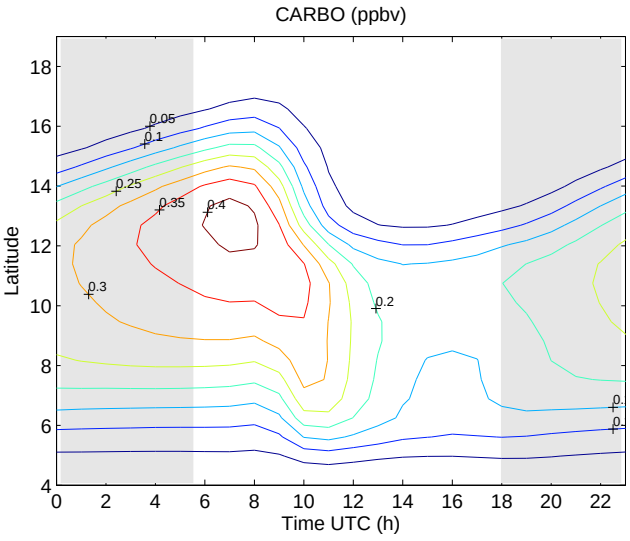

Fig. 9. Hovmöller diagram of the daily composite of the simulated CARBO mixing ratios below 700 m in ppbv. The composite is done for the last five days of simulation for the BASE run. Night time is shaded in grey.

5.3 Ozone tendencies below 700 m

Figure 10 presents the 24 h average of the ozone tendencies (convection, turbulence and chemical production) in the layer 0–700 m. It also shows the simulated meridional ozone concentration (black dashed line). Table 5 provides details of the relative contributions of the aforementioned tendencies as well as the contributions of advection for three regions. These regions are defined according to the soil cover: the 5–12° N region corresponds to the vegetated zone, the 12–16° N to the bare soils and the 16–20° N to a part of the desert.

As mentioned previously, convection acts as a source of ozone by bringing ozone-rich air from the free troposphere to the boundary layer within the downdrafts. Convection has a significant effect on the ozone conentrations south of 12° N (Table 5) with its maximum effect at 10–12° N. Consequently convection cannot drive the establishment of the modelled ozone gradient in the layer 0–700 m.

We find that ozone is chemically destroyed over the ocean where NO_x concentrations are low. These results are similar to those found by Stickler et al. (2007) over the Atlantic Ocean near the Guyanas. North of 5° N, the net ozone chemical production is positive with values in the range of 0.2–0.7 ppbv/h depending on the latitude (Fig. 10). Higher O_3 chemical production is collocated with higher NO_x mixing ratios (Fig. 8f). This suggests that ozone is under a NO_x-

Table 5. Relative contributions of chemistry, convection, turbulence and advection to the ozone tendencies during daytime, nighttime as well as 24 h averages for the three regions described in the text. These values are derived from the mean tendencies calculated over the last five days of simulation.

	5° N–12° N			12° N–16° N			16° N–20° N		
	day	night	24 h	day	night	24 h	day	night	24 h
chemistry	0.58	−0.07	0.26	1.37	−0.12	0.63	0.32	−0.02	0.15
convection	0.14	0.15	0.14	0.02	0.05	0.04	0.08	−0.005	0.04
turbulence (deposition)	−0.41	−0.34	−0.37	−0.16	−0.13	−0.15	−0.30	−0.14	−0.22
horiz. adv.	−0.28	−0.05	−0.16	0.19	0.10	0.15	0.76	0.56	0.67
vert.adv.	0.27	0.03	0.15	−0.59	−0.57	−0.58	−0.73	−0.49	−0.61
total adv.	−0.005	−0.012	−0.01	−0.39	−0.48	−0.43	−0.02	0.07	0.05
total tend.	0.30	−0.27	0.02	0.84	−0.68	0.08	0.14	−0.10	0.02

limited regime. During day time, the net O_3 production rate reaches on average 1.37 ppbv/h over bare soils, which is twice that over vegetation (Table 5). Therefore, the higher ozone production over bare soils contributes to the ozone maximum and gradient.

The turbulent tendency sign gives information on the net budget for chemical species at the surface in terms of emissions and vertical mixing (i.e. = emission rate – deposition rate). For ozone, the turbulent tendency is negative which reveals a strong effect of dry deposition. This effect is stronger over vegetation because a higher deposition velocity is assumed there (Table 4). Deposition removes up to 0.40 ppbv/h of O_3 over vegetation (Table 5) and only 0.13–0.30 ppbv/h north of 12° N. This sink almost balances the ozone net chemical production and the source from convection in the vegetated region. Dry deposition appears to be the most important mechanism in the establishment of the low O_3 mixing ratios south of 12° N .

It is worth noting that the maxima in ozone mixing ratios and ozone chemical tendency are 1° apart (Fig. 10). This difference might be explained by the northward advection of ozone by the monsoon flux as discussed previously. The positive (negative) horizontal advection of O_3 to the north (south) of 12° N supports this explanation (Table 5).

The study of the ozone tendencies suggests that both greater deposition over trees and higher ozone production to the north contribute to creating the ozone gradient by decreasing concentrations south of 12° N and increasing them to the north, respectively. Questions remain regarding firstly the relative contributions of the precursors involved in the ozone production and secondly the relative contributions of deposition and chemical production.

Below 700 m, in relatively high NO conditions, the reactions of the peroxy radicals with NO dominate over those with HO_2 as said in Sect. 4.4. These reactions with NO yield NO_2 promoting photochemical production of O_3. We aim here to assess which peroxy radicals are most involved in the O_3 production. We analyse the loss rates of NO due to its reaction with HO_2 and five peroxy radicals at 12:00 UTC when these radical concentrations maximize. HO_2 comes mainly from the photolysis of species, such as O_3 and HCHO, and the oxidation of CO. The oxidation of hydrocarbons also yields HO_2. The five peroxy radicals considered are: BIOP (peroxy radicals formed from BIO), CARBOP (acetyl peroxy radicals and peroxy radicals formed from KET, CARBO and ALD), ALKAP (peroxy radical formed from ALKA and OP2), ALKEP (peroxy radical formed from ALKE) and MO2 (methyl peroxy radical formed from CH_4 and OP1). The NO loss rates for these reactions are defined as the NO reaction rate constant for a specific radical multiplied by the radical and NO concentrations. Figure 11 presents the mean NO loss rates for the layer 0–700 m for its reaction with these six radicals as evaluated at 12:00 UTC on the 26th day of the simulation. South of 14° N, the reaction of NO with BIOP is dominant as expected with up to 1 ppbv h^{-1}. The reaction of NO with HO_2 yields around 0.4 ppbv h^{-1}. The four other radicals contribute less than 0.15 ppbv h^{-1} south of 12° N. Consequently ozone production is mostly the result of BIO oxidation over vegetation. At 14° N BIOP does not contribute much while the reaction of NO with HO_2 is dominant (with more than 1.8 ppbv h^{-1}). ALKAP and MO2 lead to around 0.5 ppbv h^{-1} each and ALKEP and CARBOP to less than 0.2 ppbv h^{-1}. At 16° N, where O_3 production is at a maximum, MO2 contributes 0.5 ppbv b^{-1}, ALKAP and CARBOP to less than 0.2 ppbv h^{-1}. Consequently the three main radicals involved in ozone formation north of the vegetated area are HO_2, MO2 and ALKAP. KET and CARBO from which CARBOP is formed are of secondary importance north of 12° N.

6 Sensitivity of ozone distribution and gradient below 700 m to emissions and dry deposition

This section investigates the influence of emissions of ozone precursors (NO_x, VOCs, CH_4) and dry deposition to the ozone distribution (Sect. 6.1 to 6.7). Figure 8, in which the

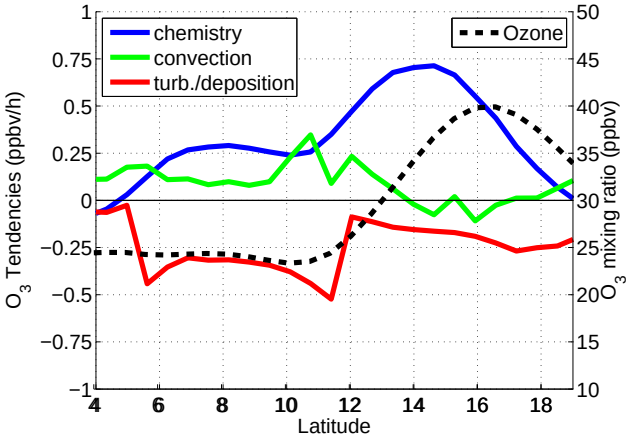

Fig. 10. 24 h-average meridional profiles of O_3 and its chemical, convective and turbulent tendencies in the layer 0–700 m in ppbv and ppbv h^{-1} between 4° N and 19° N for the BASE run.

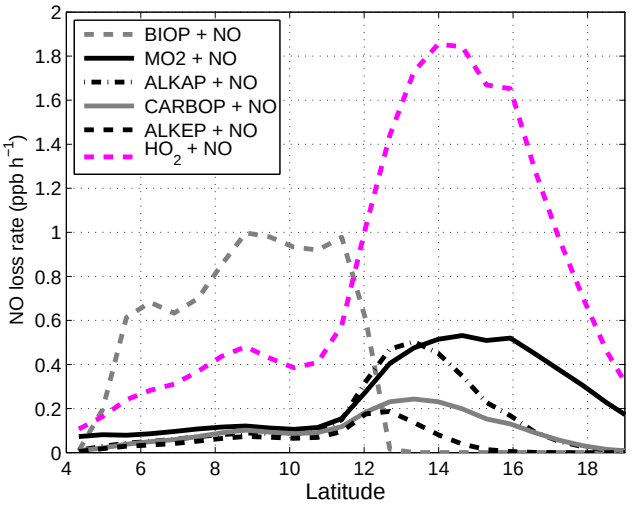

Fig. 11. Mean NO loss rates for its reaction with the peroxy radicals: HO_2, BIOP, CARBOP, ALKAP, ALKEP and MO2 on the 26th day of simulation at 12:00 UTC below 700 m between 4° N and 19° N for the BASE run in ppbv h^{-1}.

meridional profiles of the trace gases below 700 m for the BASE run were presented, also shows these profiles for the sensitivity tests. Table 6 presents the concentrations of ozone obtained at its minimum and maximum as well as the ozone gradient for each simulation. These values are derived from the profiles shown in Fig. 8.

6.1 Influence of lightning

Including NO from lightning (thereafter LNO_x) has no significant influence on the NO_x mixing ratio in the boundary layer as the production only takes place in the updrafts of the convection scheme. However an ozone increase in the UT due to LNO_x leads to an O_3 increase in the LT via the transport of ozone by the downdrafts in the convective systems (Fig. 10). Thus including LNO_x increases the ozone mixing ratio by ∼2 ppbv in the boundary layer (not shown). However this increase is uniform in latitude so it does not contribute to creating the observed ozone gradient. This slight increase of ozone when including lightning NO_x production leads to higher OH concentrations, but changes in BIO or CO through oxidation are not significant (50 ppt and 2–3 ppbv, i.e. 3% and 1.5%, respectively).

6.2 Influence of anthropogenic emissions (NOANT run)

The results from the NOANT run are represented with the red line in Fig. 8. As explained in the model description section, the BAe-146 flew mostly over low population density areas except near Niamey and the Guinea Coast. The averaged RETRO emissions between 5° W and 5° E showed that most pollutants are emitted near the Guinea Coast thus higher emission rates were prescribed between 5° N and 8° N than between 8° N and 14° N. As a consequence the greatest changes in CO and especially in NO_x are simulated below 12° N (Fig. 8d, f). Including anthropogenic emissions increases CO mixing ratios by 30–35% and leads to a better representation of the CO concentrations, but as discussed previously, even with these emissions the model underestimates the observed CO concentrations. NO_x mixing ratios increase essentially south of 11° N with up to 50% difference. The change in ozone is mostly seen south of 12° N (with a difference of up to 10%). A slight increase of 3% is simulated at 17° N which corresponds to an increase of 1–3 ppbv. These results are similar to those found with the global model ECHAM5-MOZ (Aghedo et al., 2007) in which the impact of anthropogenic emissions on surface ozone ranges from 2 to 5 ppbv over West Africa during the boreal summer season (Nigeria excluded). Adding anthropogenic emissions leads to a change in the atmospheric oxidation capacity over West Africa and BIO concentrations decrease by 20% (Fig. 8a). The shape of the meridional profile of surface ozone over vegetation is significantly modified by anthropogenic emissions: the lower values are not as well-marked as those observed and the gradient between ocean and land is not well reproduced when including anthropogenic emissions. The idealized two step distribution considered for anthropogenic emissions does not allow the model to reproduce the local pollution sampled over Cotonou (6–7° N) and Niamey (12–13° N) well. However these results indicate no significant contribution of anthropogenic emissions to the establishment of the ozone gradient (Table 6).

6.3 Influence of NO_x from wetted soils to the north (IDSOL run)

In the BASE run, higher NO_x emissions from soils are assumed north of 13° N as a consequence of the response

Table 6. Minimum (∼11° N) and maximum (∼16° N) ozone concentrations and the ozone gradient in ppbv for each run. The values are derived from the meridional profiles shown in Fig. 8. Numbers in brackets indicate the changes relatively to the BASE run.

RUN Name	O_3 min (ppbv) ∼11° N	O_3 max (ppbv) ∼16° N	O_3 gradient (ppbv)
BASE run	23	40	17
NOANT	21 (−2)	38 (−2)	17 (=)
NOISO	24 (+1)	36 (−4)	12 (−5)
IDSOL	23 (=)	33 (−7)	10 (−7)
NOCH4	20 (-3)	31 (−9)	11 (−6)
NNVOC	23 (=)	40 (=)	17 (=)
NSVOC	23 (=)	35 (−5)	12 (−5)
NODEP	34 (+11)	46 (+6)	12 (−5)

of bare soils to precipitation. The NO_x emission fluxes considered in the BASE run and which are adapted from the POET /GEIA inventory and Jaeglé et al. (2005) (2×10^{10} and 4.5×10^{10} molecules $cm^{-2}\,s^{-1}$, respectively) are in the range of the flux calculated as part of AMMA by Stewart et al. (2008) (5.1–11.2 ng N $m^{-2}\,s^{-1}$ i.e. 2.2–4.8×10^{10} molecules $cm^{-2}\,s^{-1}$) and Delon et al. (2008) (2–35 ng N $m^{-2}\,s^{-1}$ i.e. 1–15×10^{10} molecules $cm^{-2}\,s^{-1}$). Varying the NO_x flux in the 2-D model will change the ozone level. However, the chosen values for the BASE run seem to be appropriate to reproduce the average ozone and NO_x levels observed below 700 m.

In the IDSOIL run (Fig. 8, blue line), the NO_x emission fluxes are equal to 0.17×10^{10} molecules $cm^{-2}\,s^{-1}$ north and south of 12° N. The NO_x mixing ratios drop to 300 ppt at 15° N. However a maximum of NO_x is still simulated over bare soils probably due to the combination of transport by the monsoon flux and conversion from the PAN reservoir. Changing this NO_x source changes the O_3 distribution in the middle troposphere as well as the surface ozone mixing ratios south of 12° N by very little (less than 1 ppbv for the mean daytime values). In contrast, the surface O_3 mixing ratio decreases by up to 7 ppbv near the O_3 maximum (Table 6). An ozone gradient of about 10 ppbv is still simulated in the IDSOIL run. However it is not as sharp as that in the BASE run. There is almost no change in the distribution of the hydrocarbons: a 2–4% increase is simulated due to a slight decrease in OH. Assuming higher emissions of NO_x from the bare soils leads to an increase in O_3 mixing ratio of 7 ppbv and better agreement with observations.

6.4 Influence of isoprene and terpenes (NOISO run)

A sensitivity study has been performed to investigate the role of isoprene and terpenes on the ozone chemistry in the BL. Turning off the emissions of the BIO species in the model severly affects both the amount of VOCs in the troposphere and the oxidative capacity of the atmosphere. Due to non-linear effects, it is difficult to estimate the contribution of isoprene to tropospheric chemistry. Pfister et al. (2008) have used a tagging chemical scheme to quantify the impact of isoprene on species containing carbon (such as CO and HCHO) and also to assess the impact of non-linearity. However, the use of a tagging scheme is limited and can not resolve species such as OH, O_3 or NO_x. To discuss the impact on ozone in this study we use a run called NOISO in which the source of the lumped BIO species is switched off (green line Fig. 8). It is worth noting that other biogenic hydrocarbons such as alkanes, acetone or alcohols are also directly emitted by vegetation (see Table 3).

When isoprene and terpene emissions are switched off, the CARBO species, which mainly results from the BIO oxidation, is clearly not produced by the chemical scheme. KET, HCHO and CO mixing ratios decrease by 60–75% (0.5–1.5 ppbv), 40–45%(0.2–0.6 ppbv), 10–15%(10–15 ppbv) respectively when excluding isoprene and terpene. Granier et al. (2000) using a colouring technique have found that isoprene (terpenes) contribute 15–20 (3–4) ppbv of surface CO over West Africa. In the Pfister et al. (2008) tagging study, the contribution of isoprene to the CO (HCHO) column ranges around 13–15% (40–50%) in West Africa and the authors stated that they found similar contributions to the surface mixing ratios. The non-linearity effect will lead to slightly larger (smaller) changes in CO (HCHO) as explained by Pfister et al. (2008). Also different isoprene inventories can change CO surface mixing ratios by about ±20% (Pfister et al., 2008). Our results are thus in the range of the values from previous studies.

Surprisingly ozone appears to be less influenced by the BIO chemistry over vegetation than it is north of the vegetated area where O_3 changes by up to 5 ppbv. This ozone change is similar to that found in global studies. Wang and Eltahir (2000) assessed the ozone changes when they included isoprene emissions in their chemistry transport model (CTM) and found an increase of up to 8 ppbv in the surface ozone mixing ratio over West Africa. Small changes in ozone on a global scale are simulated by Pfister et al. (2008). However, they stated that regional differences in surface ozone were large (up to 5 ppbv) and that the largest absolute increase of column ozone was simulated over Equatorial Africa.

We found that the ozone chemical tendency decreases slightly over vegetation when including isoprene. In fact, including BIO emissions leads to a slight decrease of NO_x mixing ratio because of PAN formation. During daytime, the mean simulated values for PAN range from 0.01–0.05 ppt (0.1–0.3 ppt) with (without) BIO emissions in agreement with the global study of Wang and Eltahir (2000). The thermal decomposition of PAN at 300 K leads to an approximate lifetime of 30 min for PAN. Despite the importance of the PAN decompostion, enough carbonyl radicals (called CARBOP) are available in the middle of the day to balance the low values of NO_x and lead to PAN formation. This chemical behaviour has been reported in previous studies: i.e. Singh et al. (1990) and Jacob and Wofsy (1990) during the wet season experiment in Amazonia ABLE2B and Doskey et al. (2004) over grassland in Illinois. As a consequence of the conversion of NO_x to PAN over vegetation and northward transport by the monsoon flux, the additional "fuel" provided by BIO emissions leads to decreased NO_x concentrations over trees while increasing them north of 14° N. As the ozone regime is NO_x-limited, including BIO may thus decrease the ozone chemical production over vegetation.

The ozone maximum decrease by 5 ppbv when BIO emissions are switched-off. The ozone chemical production seems sensitive to the amount of VOCs available in spite of the NO_x-limited regime for ozone. Without BIO emissions, VOC amounts available north of the vegetated area is clearly diminish. This shows that the secondary hydrocarbons and longer-lived products (CO, HCHO) are transported by the monsoon flux north of the vegetated area where they are oxidized and contribute to the ozone maximum.

6.5 Influence of the VOCs (NNVOC and NSVOC runs)

Whereas the IDSOL, NOANT and NOISO runs assessed the influence of sources by category (anthropogenic and biogenic), this section aims to assess whether the VOCs that are directly emitted north of 12° N (anthropogenic only) have more impact on the ozone maximum than the VOCs emitted south of 12° N (both biogenic and anthropogenic). Two runs are used to answer that: the run NNVOC (red dashed line) in which the VOC emissions north of 12° N are switched off and the run NSVOC (green dashed line) in which the VOC emissions south of 12° N are switched off.

The VOCs emitted north of 12° N (NNVOC) have no significant impact on the ozone levels of gradient, but shifts the ozone maximum slightly to the north. Switching-off VOC emissions south of 12° N (NSVOC) has a similar effect to switching-off isoprene emissions (which is the majority of the VOC emissions): only ozone levels north of the vegetated areas are impacted. The ozone maximum decreases by 5 ppbv and is slighly shifted to the north. Similar to the results of the NOISO run, the northward advection of materials (such as secondary products and longer lived species) is a mechanism that plays a substantial role in the establishment of the ozone gradient.

6.6 Influence of background CH_4 (NOCH4 run)

In this section the influence of the background methane which is constrained at 1800 ppbv in the model, is investigated. In the NOCH4 run (grey line), the methane concentrations are set to zero. Omitting CH_4 decreases the MO2 radical concentrations by a half to two thirds of the levels in the base run, and HO_2 by ∼13% at 15° N (not shown). CH_4 is the major contributor to MO2 formation, especially in the north where MO2 reaches its maximum (16° N). Without CH_4, ozone concentrations decrease both north and south of 12° N by ∼9 ppbv and ∼3 ppbv, respectively (Fig. 8, grey line). CH_4 increases the ozone gradient by ∼6 ppbv (Table 6) similar to the relative influence of the BIO species or the VOCs from the south of 12° N.

6.7 Influence of ozone dry deposition over trees (NODEP run)

Ozone deposition is the major sink for ozone over vegetation. The sensitivity test called NODEP (dashed grey line) was performed to assess the contribution of dry deposition to the lower ozone mixing ratios between 5° N and 12° N. In the NODEP run, O_3 dry deposition was omitted from the whole domain.

When we compare the BASE and the NODEP runs, we can see that O_3 dry deposition leads to a loss of about 3–4, 5–10 and 5 ppbv of surface O_3 over ocean, vegetation and bare soils/desert, respectively (Fig. 8 grey dashed line). The largest influence is seen over vegetation where the dry deposition velocity of ozone was assumed to be higher. Deposition decreases the oxidation capacity of the atmosphere by lowering the O_3 and subsequently OH levels, so that CO and BIO are oxidized less (2–3 ppbv and 300 ppt, respectively). Including O_3 deposition allows the low ozone concentrations observed over the vegetation and a significant gradient to the north to be simulated. Moreover, the O_3 concentrations obtained over vegetation without deposition are clearly higher than those from the others simulation (Table 6). This shows that deposition is the main factor that controls the low concentrations of ozone over vegetation.

7 Conclusions

Well marked meridional gradients in trace gas concentrations have been observed during the wet season in the lower troposphere of West Africa during the AMMA 2006 campaign. These horizontal variations are related to the latitudinal variations of the land cover in West Africa which leads to emission and deposition changes with latitude. A two dimensional model (latitude vs. altitude) has been used to determine which processes are involved in creating these

gradients. Idealized latitudinal distributions of emission fluxes have been adapted from various emission inventories to account for both natural and anthropogenic emissions.

The model reproduces the observed lower tropospheric latitudinal variation in ozone extremely well along with the spatial distribution and magnitude of biogenic compounds and nitrogen oxides. Higher concentrations of isoprene and CO are both observed and simulated over the vegetated area (5° N–12° N) compared to the region north of 12° N. North of 12° N, pulses of NO emissions from recently wetted soils have been observed during the AMMA campaing (Stewart et al., 2008) and have been related to enhancement of PAN and O_3 concentrations (Stewart et al., 2008; Delon et al., 2008). We assumed higher NO emissions from soils between 12° N and 16° N to simulate this feature. Consequently modelled NO_x mixing ratios reach a mean value of 0.6 ppbv over bare soils below 700 m, while they stay below 0.3 ppbv over vegetation.

The main aim of the paper is to assess the factors controlling the ozone distribution in the layer 0–700 m. Indeed, below 700 m both observation and model show that the O_3 mixing ratios are lower than 25 ppbv over vegetation while they reach a maximum of 40 ppbv (and more) at 16° N. The model simulates a 17 ppbv gradient of ozone between the vegetated area and the Sahelian region. The different locations of the Guinean coast in the model (5° N) and at the locations of the observations (6° N) lead to an overestimation of the ozone precursors south of 6–7° N. Also VOCs are overestimated north of 12° N because emissions from vegetation are constant to this limit, whereas in reality they become somewhat patchy in the region over-flown by the aircraft. The meridional profiles of the trace gases are overall compared well to the observations, allowing further analysis.

The model diagnostics show that convection brings O_3-rich air from the free troposphere to the BL in downdrafts, but this process has no role in the establishment of the ozone gradient. We found that the lower values of ozone over vegetation are essentially controlled by dry deposition over trees and that the ozone maximum is clearly a consequence of higher NO_x mixing ratios north of 12° N. Indeed, the largest impact on the minimum is from dry deposition over vegetation (11 ppbv) and the largest change on the gradient (∼7 ppbv) comes from the difference in NO_x emissions (and concentrations) between the north and the south of 12° N. The chemistry regime for ozone is found to be NO_x-limited with a net chemical production of 0.25 ppbv h^{-1} over vegetation and up to 0.75 ppbv h^{-1} over bare soils. The ozone production in the north requires carbonated fuel that comes from background CO and CH_4 as well as VOCs emitted by biogenic and anthropogenic sources. A sensitivity test showed that background methane contributes to the ozone gradient with an amount of ∼6 ppbv. This contribution is similar to that from biogenic VOCs emitted south of 12° N. These results indicate a significant role of the northward advection of materials. Longer-lived or secondary VOCs produced from the oxidation of biogenic species contribute ∼5 ppbv to the establishment of the ozone gradient. The other sources (lightning and anthropogenic) modify the ozone levels to some extent but do not contribute to the ozone gradient.

A case study based on the observations made during the B219A and B219B flights, should help to further analyse the isoprene chemistry over West African forests and savannas and to confirm the contribution of the northward advection of biogenic species to the ozone formation further north of the area of their emissions.

Acknowledgements. Based on an French initiative, AMMA was built by an international scientific group and is currently funded by a large number of agencies, especially from France, the United Kingdom, the United States, and Africa. It has been the beneficiary of a major financial contribution from the European Communities Sixth Framework Research Programme. Detailed information on scientific coordination and funding is available on the AMMA International Web site at http://www.amma-international.org. Computer time has been provided by the Institut du Développement et des Ressources en Informatique Scientifique (IDRIS). This work was partly funded by the UK Natural Environment Research Council through tha AMMA-UK Consortium grant and received support from the National Centre for Atmospheric Science (NCAS), including Facility for Airborne Atmospheric Measurements and the British Atmospheric Data Centre. We thank the anonymous referee for their constructive and fruitful comments that help to significantly improve the manuscript.

Edited by: F. Dentener

The publication of this article is financed by CNRS-INSU.

References

Aghedo, A. M., Schultz, M. G., and Rast, S.: The influence of African air pollution on regional and global tropospheric ozone, Atmos. Chem. Phys., 7, 1193–1212, 2007, http://www.atmos-chem-phys.net/7/1193/2007/.

Andrea, M., Chapuis, A., Cros, B., Fontan, J., Helas, G., Justice, C., Kaufman, Y., Minga, A., and Nganga, D.: Ozone and Aitken nuclei over Equatorial Africa: Airborne observations during DECAFE 88, J. Geophys. Res., 97, 6137–6148, 1992.

Baumbach, G., Vogt, U., Hein, K., Oluwole, A., Ogunsola, O., Olaniyi, H., and Akeredolu, F.: Air pollution in a large tropical city with a high traffic density – results of measurements in Lagos, Nigeria, Sci. Total Environ., 169, 25–31, doi:10.1016/0048-9697(95)04629-F, 1995.

Bechtold, P., Bazile, E., Guichard, F., Mascart, P., and Richard, E.: A mass-flux convection scheme for regional and global models, Q. J. Roy. Meteor. Soc., 127, 869–886, 2001.

Bond, D. W., Steiger, S., Zhang, R., Tie, X., and Orville, R.: The importance of NO_x production by lightning in the tropics, Atmos. Environ., 36(9), 1509–1519, 2002.

Bougeault, P. and Lacarrère, P.: Parametrization of orography induced turbulence in a mesobeta-scale model, Mon. Weather Rev., 117, 1872–1890, 1989.

Butler, T. M., Taraborrelli, D., Brühl, C., Fischer, H., Harder, H., Martinez, M., Williams, J., Lawrence, M. G., and Lelieveld, J.: Improved simulation of isoprene oxidation chemistry with the ECHAM5/MESSy chemistry-climate model: lessons from the GABRIEL airborne field campaign, Atmos. Chem. Phys., 8, 4529–4546, 2008,
http://www.atmos-chem-phys.net/8/4529/2008/.

Cardenas, L. M., Brassington, D. J., Allan, B. J., Coe, H., Alicke, B., Platt, U., Wilson, K. M., Plane, J. M. C., and Penkett, S. A.: Intercomparison of formaldehyde measurements in clean and polluted atmospheres, J. Atmos. Chem., 37, 53–80, 2000.

Christian, H., Blakslee, R., Boccippio, D., Boek, W., Buechler, D., Driscoll, K., Goodman, S., Hall, J., Koshak, W., Mach, D., and Stewart, M.: Global frequency and distribution of lightning as observed by the Optical Transient Detector, J. Geophys. Res., 108(D1), 4005, doi:10.1029/2002JD002347, 2003.

Crassier, V., Shure, K., Tulet, P., and Rosset, R.: Development of a reduced chemical scheme for use in mesoscale meteorological models, Atmos. Environ., 34, 2633–2644, 2000.

Cros, B., Fontan, J., Minga, A., Helas, G., Nganga, D., Delmas, R., Chapuis, A., Benech, B., Druilhet, A., and Andrea, M.: Vertical profiles of ozone between 0 and 400 m in and above an African Equatorial forest, J. Geophys. Res., 97, 12877–12877, 1992.

Cros, B., Delon, C., Affre, C., Marion, T., Druilhet, A., Perros, P., and Lopez, A.: Sources and sinks of ozone in savanna forest areas during EXPRESSO: Airborne turbulent flux measurements, J. Geophys. Res., 105, 29347–29358, 2000.

Cuxart, J., Bougeault, P., and Redelsperger, J.-L.: A turbulence scheme allowing for mesoscale and large-eddy simulations, Q. J. Roy. Meteor. Soc., 126, 1–30, 2000.

DeCaria, A., Pickering, K., Stenchikov, G., and Ott, L.: Lightning-generated NO_x and its impact on tropospheric ozone production: A three dimensional modeling study of a Stratosphere-Troposphere Experiment: Radiation, Aerosols and Ozone (STERAO-A) thunderstom, J. Geophys. Res., 110, D14303, doi:10.1029/2004JD005556, 2005.

Delon, C., Reeves, C. E., Stewart, D. J., Serça, D., Dupont, R., Mari, C., Chaboureau, J.-P., and Tulet, P.: Biogenic nitrogen oxide emissions from soils – impact on NO_x and ozone over West Africa during AMMA (African Monsoon Multidisciplinary Experiment): modelling study, Atmos. Chem. Phys., 8, 2351–2363, 2008,
http://www.atmos-chem-phys.net/8/2351/2008/.

Doskey, P., Kotamarthi, V., Fukui, Y., Cook, D., Breitbeil, F., and Wesly, M.: Air-surface exchange of peroxyacetyl nitrate at grassland site, J. Geophys. Res., 109, D10310, doi:10.1029/2004JD004533, 2004.

Fan, S.-M., Wofsy, S., Bakwin, P., Jacob, D., and Fitzjarrald, D.: Atmopshere-Biosphere Exchange of CO_2 and O_3 in the Central Amazon Forest, J. Geophys. Res., 95, 16851–16864, 1990.

Fanou, L., Mobio, T., Creppy, E., Fayomi, B., Fustoni, S., Moller, P., Kyrtopoulos, S., Georgiades, P., Loft, S., Sanni, A., Skov, H., Ovrebo, S., and Autrup, H.: Survey of air pollution in Cotonou, Benin – air monitoring and biomarkers, Sci. Total Environ., 358, 85–96, doi:10.1016/j.scitotenv.2005.03.025, 2006.

Gerbig, C., Schmitgen, S., Kley, D., Volz-Thomas, A., Dewey, K., and Haaks, D.: An improved fast-response vacuum UV resonance fluorescence CO instrument, J. Geophys. Res., 104, 1699–1704, 1999.

Granier, C., Pétron, G., Müller, J.-F., and Brasseur, G.: The impact of natural and anthropogenic hydrocarbons on the tropospheric budget of carbon monoxide, Atmos. Environ., 34, 5255–5270, 2000.

Granier, C., Lamarque, J. F., Mieville, A., Müller, J. F., Olivier, J., Orlando, J., Peters, J., Petron, G., and Tyndall, G.: POET, a database of surface emissions of ozone precursors, online available at: http://www.aero.jussieu.fr/projet/ACCENT/POET.php, 2005.

Gregory, G., Browell, E., and Warren, L.: Boundary-layer ozone – an airborne survey above the Amazon Basin, J. Geophys. Res., 93, 1452–1468, 1988.

Guenther, A.and Hewitt, C. N., Erickson, D., Fall, R., Geron, C., Graedel, T., Harley, P., Klinger, L., Lerdau, M., McKay, W. A., Pierce, T., Scholes, B., Steinbrecher, R., Tallamraju, R., Taylor, J., and Zimmerman, P.: A global model of natural volatile organic compound emissions, J. Geophys. Res., 100, 8873–8892, 1995.

Hopkins, J. R., Evans, M. J., Lee, J. D., Lewis, A. C., Marsham, J. H., McQuaid, J. B., Parker, D. J., Stewart, D. J., Reeves, C. E., and Purvis, R. M.: Direct estimates of emissions from the megacity of Lagos, Atmos. Chem. Phys. Discuss., 9, 8667–8682, 2009,
http://www.atmos-chem-phys-discuss.net/9/8667/2009/.

Jacob, D. J. and Wofsy, S. C.: Budgets of Reactive Nitrogen, Hydrocarbons and Ozone Over the Amazon Forest during the Wet Season, J. Geophys. Res., 95, 16737–16754, 1990.

Jaeglé, L., Martin, R., Chance, K., Steinberger, L., Kurosu, T., Jacob, D., Modi, A., Yobou, V., Sigha-Nkamdjou, L., and Galy-Lacaux, C.: Satellite mapping of rain-induced nitric oxide emissions from soils, J. Geophys. Res., 109, D21310, doi:10.1020/2004JD004787, 2004.

Jaeglé, L., Steinberger, L., Martin, R., and Chance, K.: Global partitionning of NO_x sources using satellite observations: relative roles of fossil fuel combustion, biomass burning and soils emissions, Faraday Discuss., 130, 1–17, 2005.

Janicot, S., Thorncroft, C. D., Ali, A., Asencio, N., Berry, G., Bock, O., Bourles, B., Caniaux, G., Chauvin, F., Deme, A., Kergoat, L., Lafore, J.-P., Lavaysse, C., Lebel, T., Marticorena, B., Mounier, F., Nedelec, P., Redelsperger, J.-L., Ravegnani, F., Reeves, C. E., Roca, R., de Rosnay, P., Schlager, H., Sultan, B., Tomasini, M., Ulanovsky, A., and ACMAD forecasters team: Large-scale overview of the summer monsoon over West Africa during the AMMA field experiment in 2006, Ann. Geophys., 26, 2569–2595, 2008,
http://www.ann-geophys.net/26/2569/2008/.

Jonquière, I., Marenco, A., Maalej, A., and Rohrer, F.: Study of ozone formation and transatlantic transport from biomass burning emissions over West Africa during the airborne Tropospheric Ozone Campaigns TROPOZ I and TROPOZ II, J. Geophys. Res., 103, 19059–19073, 1998.

Kesselmeier, J. and Staudt, M.: Biogenic organic volatile compounds (VOCs): An overview of emission, physiology and ecol-

ogy, J. Atmos. Chem., 33, 23–88, 1999.

Kirchhoff, V., Browell, E., and Gregory, G.: Ozone measurements in the troposphere of an Amazonian rain forest environment, J. Geophys. Res., 93, 15850–15860, 1988.

Krol, M. C., Molemaker, M. J., and de Arellano, J. V. G.: Effects of turbulence and heterogeneous emissions on photochemically active species in the convective boundary layer, J. Geophys. Res., 105, 6871–6884, 2000.

Labrador, L. J., von Kuhlmann, R., and Lawrence, M. G.: The effects of lightning-produced NO_x and its vertical distribution on atmospheric chemistry: sensitivity simulations with MATCH-MPIC, Atmos. Chem. Phys., 5, 1815–1834, 2005, http://www.atmos-chem-phys.net/5/1815/2005/.

Lafore, J. P., Stein, J., Asencio, N., Bougeault, P., Ducrocq, V., Duron, J., Fischer, C., Héreil, P., Mascart, P., Masson, V., Pinty, J. P., Redelsperger, J. L., Richard, E., and Vilá-Guerau de Arellano, J.: The Meso-NH Atmospheric Simulation System. Part I: adiabatic formulation and control simulations, Ann. Geophys., 16, 90–109, 1998, http://www.ann-geophys.net/16/90/1998/.

Lawrence, M., von Kuhlmann, R., and Salzmann, M.: The balance of effects of deep convective mixing on tropospheric ozone, Geophys. Res. Lett., 30(18), p. 1940, 2003.

Lelieveld, J., Butler, T., Crowley, J. N., Dillon, T. J., Fisher, H., Ganzeveld, L., Harder, H., Lawrence, M. G., Martinez, M., Taraborrelli, D., and Williams, J.: Atmospheric oxidation capacity sustained by a tropical forest, Nature, 452, 737–740, doi:10.1038/nature06870, 2008.

Linden, J., Thorsson, S., and Eliasson, I.: Carbon Monoxide in Ouagadougou, Burkina Faso – A comparison between urban background, roadside and in-traffic measurements, Water Air Soil Pollut., 188, 345–353, doi:10.1007/s11270-007-9538-2, 2008.

Mahfouf, J.-F. and Noilhan, J.: Inclusion of gravitational drainage in a land surface scheme based on the forced-restore method, J. Appl. Meteorol., 35, 987–992, 1996.

Mari, C., Jacob, D., and Bechtold, P.: Transport and scavenging of soluble gases in deep convection cloud, J. Geophys. Res., 105, 22255–22267, 2000.

Mari, C., Chaboureau, J. P., Pinty, J. P., Duron, J., Mascart, P., Cammas, J. P., Gheusi, F., Fehr, T., Schlager, H., Roiger, A., Lichtenstein, M., and Stock, P.: Regional lightning NO_x sources during the TROCCINOX experiment, Atmos. Chem. Phys., 6, 5559–5572, 2006, http://www.atmos-chem-phys.net/6/5559/2006/.

Mari, C. H., Cailley, G., Corre, L., Saunois, M., Attié, J. L., Thouret, V., and Stohl, A.: Tracing biomass burning plumes from the Southern Hemisphere during the AMMA 2006 wet season experiment, Atmos. Chem. Phys., 8, 3951–3961, 2008, http://www.atmos-chem-phys.net/8/3951/2008/.

Martin, R. V., Jacob, D. J., Logan, J. A., Ziemke, J. M., and Washington, R.: Detection of a lightning influence on tropical tropospheric ozone, Geophys. Res. Lett., 27(11), 1639–1642, 2000.

Martin, R. V., Sauvage, B., Folkins, I., Sioris, C. E., Boone, C., Bernath, P., and Ziemke, J.: Space-based constraints on the production of nitric oxide by lightning, J. Geophys. Res., 112, D09309, doi:10.1020/2006JD007831, 2007.

Matsuda, K., Watanabe, I., Wingpud, V., Theramongkol, P., and Ohizimi, T.: Deposition velocity of O_3 and SO_2 in the dry and wet season above a tropical forest in northern Thailand, Atmos. Environ., 40, 7557–7564, 2006.

Mondon, S. and Redelsperger, J.-L.: A study of a fair weather boundary layer in togacoare: parametrization of surface fluxes in large scale and regional models for light wind conditions, Bound.-Lay. Meteorol., 88, 47–76, 1998.

Müller, J.-F., Stavrakou, T., Wallens, S., De Smedt, I., Van Roozendael, M., Potosnak, M. J., Rinne, J., Munger, B., Goldstein, A., and Guenther, A. B.: Global isoprene emissions estimated using MEGAN, ECMWF analyses and a detailed canopy environment model, Atmos. Chem. Phys., 8, 1329–1341, 2008, http://www.atmos-chem-phys.net/8/1329/2008/.

Murphy, J., Oram, D., and Reeves, C.: PTr-MS measurements of isoprene, acetone, acetonitrile over West Africa, in preparation, Atmos. Chem. Phys. Discuss., 2009.

Parker, D., Burton, R., Diongue-Niang, A., Ellis, R., Felton, M., Tayloy, C., Thorncroft, C., Bessemoulin, P., and Tompkins, A.: The diurnal cycle of the West African monsoon circulation, Q. J. Roy. Meteor. Soc., 131, 2839–2860, 2005.

Peyrillé, P. and Lafore, J.-P.: An idealized two-dimensional framework to study the West African monsoon, part II: large scale advection and the diurnal cycle, J. Atmos. Sci., 64, 2783–2803, 2007.

Peyrillé, P., Lafore, J.-P., and Redelsperger, J.-L.: An idealized two-dimensional framework to study the West African monsoon, part I: Validation and key controlling factors, J. Atmos. Sci., 64, 2765–2782, 2007.

Pfister, G., Emmons, L., Hess, P. G., Lamarque, J.-F., Orlando, J., Walters, S., Guenther, A., Palmer, P., and Lawrence, P.: Contribution of isoprene to chemical budgets: A model tracer study with the NCAR CTM MOZART-4, J. Geophys. Res., 113, D02204, doi:10.1029/2007JD008948, 2008.

Pickering, K. E., Thompson, A. M., Wang, Y., Tao, W.-K., McNamara, D. P., Kirchhoff, V. M. J. H., Heikes, B. G., Sachse, G. W., Bradshaw, J. D., Gregory, G. L., and Blake, D. R.: Convective transport of biomass burning emissions over Brazil during TRACE A, J. Geophys. Res., 101, 23993–24012, 1996.

Price, C. and Rind, D.: A simple lightning parametrization for calculating global lightning distributions, J. Geophys. Res., 97, 9919–9933, 1992.

Price, C. and Rind, D.: What determines the cloud-to-ground lightning fraction in thunderstorm?, J. Geophys. Res., 20, 463–466, 1993.

Reeves, C., Ancellet, G., Borgon, A., Cairo, F., Mari, C., Methven, J., Schlager, H., and Thouret, V.: Chemical characterisation of the West Africa monsoon during AMMA, Atmos. Chem. Phys. Discuss., in preparation, 2009.

Reynolds, R. and Smith, W.: A high-resolution global sea surface temperatures climatology, J. Climate, 8, 1571–1583, 1995.

Rummel, U., Ammann, C., Kirkman, G. A., Moura, M. A. L., Foken, T., Andreae, M. O., and Meixner, F. X.: Seasonal variation of ozone deposition to a tropical rain forest in southwest Amazonia, Atmos. Chem. Phys., 7, 5415–5435, 2007, http://www.atmos-chem-phys.net/7/5415/2007/.

Saunois, M., Mari, C., Thouret, V., Cammas, J., Peyrillé, P., Lafore, J., Sauvage, B., Volz-Thomas, A., Nédélec, P., and Pinty, J.: An idealized two-dimensional approach to study the impact of the West African monsoon on the meridional gradient of tropospheric ozone, J. Geophys. Res., 113, D07306, doi:10.1029/2007JD008707, 2008.

Sauvage, B., Thouret, V., Cammas, J.-P., Gheusi, F., Athier, G., and Nédélec, P.: Tropospheric ozone over Equatorial Africa: regional aspects from the MOZAIC data, Atmos. Chem. Phys., 5, 311–335, 2005, http://www.atmos-chem-phys.net/5/311/2005/.

Sauvage, B., Martin, R. V., van Donkelaar, A., Liu, X., Chance, K., Jaeglé, L., Palmer, P. I., Wu, S., and Fu, T.-M.: Remote sensed and in situ constraints on processes affecting tropical tropospheric ozone, Atmos. Chem. Phys., 7, 815–838, 2007a.

Sauvage, B., Martin, R. V., van Donkelaar, A., and Ziemke, J. R.: Quantification of the factors controlling tropical tropospheric ozone and the South Atlantic maximum, J. Geophys. Res., 112, D11309, doi:10.1029/2006JD008008, 2007b.

Sauvage, B., Thouret, V., Cammas, J.-P., Brioude, J., Nédélec, P., and Mari, C.: Meridional ozone gradients in the African upper troposphere, Geophys. Res. Lett., 34, L03817, doi:10.1029/2006GL028542, 2007c.

Schultz, M., Pulles, T., Brand, R., van het Bolscher, M., and Dalsøren, S.: A global data set of anthropogenic CO, NO_x, and NMVOC emissions for 1960–2000, in preparation, 2005.

Seinfeld, J. and Pandis, S.: Atmospheric Chemistry and Physics: From Air Pollution to Climate Change, John Wiley & Sons, 19, 958–960, 1998.

Shindell, D. T., Faluvegi, G., Stevenson, D. S., Krol, M. C., Emmons, L. K., Lamarque, J.-F., Pétron, G., Dentener, F. J., Ellingsen, K., Schultz, M. G., Wild, O., Amann, M., Atherton, C. S., Bergmann, D. J., Bey, I., Butler, T., Cofala, J., Collins, W. J., Derwent, R. G., Doherty, R. M., Drevet, J., Eskes, H. J., Fiore, A. M., Gauss, M., Hauglustaine, D. A., Horowitz, L. W., Isaksen, I. S. A., Lawrence, M. G., Montanaro, V., Müller, J.-F., Pitari, G., Prather, M. J., Pyle, J. A., Rast, S., Rodriguez, J. M., Sanderson, M. G., Savage, N. H., Strahan, S. E., Sudo, K., Szopa, S., Unger, N., van Noije, T. P. C., and Zeng, G.: Multimodel simulations of carbon monoxide: Comparison with observations and projected near-future changes, J. Geophys. Res., 111, D19306, doi:10.1029/2006JD007100, 2006.

Singh, H., Herlth, D., O'Hara, D., Salas, L., Torres, A., Gregory, G., Sachse, G., and Kasting, J.: Atmospheric Peroxyacetyl Nitrate Measurements Over the Brazilian Amazon Basin During the Wet Season: Relationships With Nitrogen Oxides and Ozone, J. Geophys. Res., 95, 16945–16954, 1990.

Stewart, D. J., Taylor, C. M., Reeves, C. E., and McQuaid, J. B.: Biogenic nitrogen oxide emissions from soils: impact on NO_x and ozone over west Africa during AMMA (African Monsoon Multidisciplinary Analysis): observational study, Atmos. Chem. Phys., 8, 2285–2297, 2008, http://www.atmos-chem-phys.net/8/2285/2008/.

Stickler, A., Fischer, H., Bozem, H., Gurk, C., Schiller, C., Martinez-Harder, M., Kubistin, D., Harder, H., Williams, J., Eerdekens, G., Yassaa, N., Ganzeveld, L., Sander, R., and Lelieveld, J.: Chemistry, transport and dry deposition of trace gases in the boundary layer over the tropical Atlantic Ocean and the Guyanas during the GABRIEL field campaign, Atmos. Chem. Phys., 7, 3933–3956, 2007, http://www.atmos-chem-phys.net/7/3933/2007/.

Stockwell, W., Kirchner, F., Kuhn, M., and Seefeld, S.: A new mechanism for regional atmospheric chemistry modeling, J. Geophys. Res., 102, 25847–25879, 1997.

Thompson, A. M.: The oxidizing capacity of the Earth's atmosphere: probable past and future changes, Science, 256, 1157–1165, 1992.

Thouret, V., Saunois, M., Minga, A., Mariscal, A., Sauvage, B., Solete, A., Agbangla, D., Nédélec, P., Mari, C., Reeves, C. E., and Schlager, H.: Two years of Ozone radio soundings over Cotonou as part of AMMA: overview, Atmos. Chem. Phys. Discuss., 9, 11221–11268, 2009, http://www.atmos-chem-phys-discuss.net/9/11221/2009/.

von Kuhlmann, R., Lawrence, M., Crutzen, P., and Rasch, P.: A model for studies of tropospheric ozone and non-methane hydrocarbons: Model description and ozone results, J. Geophys. Res., 108(D9), 4294, doi:10.1029/2002JD002893, 2003.

Wang, G. and Eltahir, E.: Biosphere-atmosphere interactions over West Africa. II: Multiple climate equilibria, Q. J. Roy. Meteor. Soc., 126, 1261–1280, 2000.